A three dimensional hydrodynamic model of the Scheldt estuary for the transport of fine sediment.

Document RIKZ/OS-96.143X

Authors R.M. Salden
Z. Yang

July 1996

Ministry of Transport, Public Works and Water Management
Directorate-General for Public Works and Water Management
National Institute for Coastal and Marine Management / *RIKZ*

1.0 Introduction.

The past years the Scheldt estuary has been dealing with a lot of changes caused by human activity in the area near the harbour of Antwerpen. Construction works for new harbours as the sluices near Bath (1987), the "Waaslandhaven" with the Kallosluices (the beginning of the eighties) and the Berendrechtsluices can be mentioned. Consequently access channels had to be made for the harbours.
At the same time new policy with respect to the distribution of spoil was defined. Before 1987 the spoil from the harbourdocks and the access channels was mainly dumped in the Lower Seascheldt. In the period 1987-1990 a transition took place to the storage of spoil on land and in the deeper parts of the docks. After 1990 all the spoil was stored in this way and distribution in the Lower Seascheldt no longer took place. The basic underlying idea was that by extracting (contaminated) spoil from the Lower Seascheldt, the waterquality in the Westernscheldt could be improved.
This extraction of mud from the watersystem has been going on up to now. This must have had consequences for the amount of mud present in the Westernscheldt and for the mud balance.
In order to be able to investigate the impact of extraction of mud on the mud budget and the effects on the mud content of tidal flats, we intend to use a sediment transport model. This sediment model calculates the transport of sediment driven by the hydrodynamic conditions within the estuary.
Therefore, the first thing we should do is set up and calibrate a hydrodynamic model of the Scheldt estuary, which provides the necessary input for the sediment model. This hydrodynamic model is described in this document.

2.0 The Model.

The first choice that has to be made is whether a one -, two - or three dimensional model is used. This choice depends on the complexity of the model area. An estuary like the Westernscheldt can not be modelled sufficiently accurate with an one dimensional (1D) approach. The system shows a lot of variation in the direction perpendicular to the main current; the presence of tidal flats and the complex structure of ebb - and flood dominated tidal channels necessitates a two dimensional (2D) approach.
When the transport of sediment is concerned, it is generally not sufficient to use a 2D model. Because the vertical profile of the sediment concentration generally shows high concentrations near the bottom, the largest part of the sediment transport has to take place using the near bottom currents. Dependent on the vertical shear in the velocity field, which can be large in the Westernscheldt, the differences between a 2D and 3D model can be significant.
The vertical shear in the velocity field is important in an other aspect. In 2D models the horizontal mixing that takes place on scales smaller than the gridspace has to be parametrized by a diffusion coefficient. The value of this coefficient is difficult to estimate. The main source for this horizontal diffusion however, is the vertical shear in the velocity field. As this shear is explicitly calculated is the 3D approach, the main part of the horizontal diffusion is taken into account naturally and the diffusion coefficient can almost be given a zero value. In this way the mixing of sediment takes place in a natural way.

2.1 Description of the model area

The numerical model that is used is TRIWAQ-in-SIMONA, which is the three dimensional analogon of the well known WAQUA. The shallow water

equations are discretized and solved on a grid that is curvilinear in the horizontal direction and which uses σ-coordinates in the vertical. Detailed information about the numerical scheme and the set up of the model can be found in [Lander et al., 1995] and [Kuiper, 1993].
The horizontal grid extends from the line Westkapelle-Zeebrugge at the sea side to Rupelmonde at the river end and is shown in figure **1**. The depth chart is given in figure **2**. The resolution is 400 by 400 m in the larger part of the domain. Eastward from approximately Baalhoek, a transition to a curvilinear grid takes place. The resolution is increased and the gridlines are parallel to the current direction. In order to get the proper tidal prism and saving computer memory, a tail is added to represent the river upstream from Rupelmonde. The number of horizontal grid points 201 x 176, of which about 20% is active during the calculation (the so called wet points). This grid is known by the name SCALDIS400.
In vertical direction, 9 layers are specified which occupy a proportional part of the watercolumn. As soon as the waterdepth is less than 0.3 meters the grid cell is considered being dry.

2.2 Model parameters.

The initial model input was taken from [Lievense, 1994]. This model input was used for the 2D version of the model so some adaptions had to be made to the parameters used. In this section we will discuss these changes and will also introduce the extra parameters that had defined for the 3D simulations.
Time step which is used in the calculations is one minute. An experiment with a larger time step was performed, but this led to an instability in the transport equation. The instability is thought to be caused by the interaction of flow field and the transport of salinity.

The bed friction is quadratically dependent on the bottom velocity. For this relation a Manning coefficient is specified. This Manning coefficient was taken from the calibration of the 2D model [Lievens, 1994]. However, within the program this 2D Manning coefficient is transformed into a coefficient for the 3D model. It is this latter coefficient which is used to define the relation between the bedfriction and the bottom velocity.
The windstress is of minor importance in an estuary like the Westernscheldt. It is uniform in space and quadratically dependent on the windspeed W_{10} at ten meters above the surface, calculated using a constant dragcoefficient C_D. The windevents at the sea side opening of the estuary are assimilated into the boundary conditions.

As already mentioned, the main part of the horizontal diffusion in the model is caused by vertical shear in the velocity field, which is explicitly modelled in the 3D case. Therefore the horizontal diffusion coefficient D_h only has a small value of $D_h = 1$ m^2/s and is mainly meant to stabilize the calculations. The same argument is valid for the horizontal viscosity ν_h which is also given the value $\nu_h = 1.0$ m^2/s.

The vertical turbulent viscosity ν_z and - diffusion D_z is calculated using an algebraic turbulence model. The Prandtl mixing length model is used in combination with an algebraic equation for the turbulent kinetic energy to calculate the vertical turbulent viscosity. A factor C_μ on the vertical viscosity can be given which is the main parameter to be calibrated by comparing the vertical velocity profiles with observed data. In our simulations we ended up using a value $C_\mu = 0.20$.
The vertical turbulent diffusion is calculated from the vertical turbulent viscosity using the so called Prandtl-Schmidt number σ_z. We used the value $\sigma_z = 1.0$.
Turbulence is suppressed by stratification using Richardson-number dependent

damping functions. The Richardson number is a measure for the strength of the stratification.
More detailed information about the turbulence model can be found in the appendix A.

2.3 Boundary conditions and forcing.

The forcing of the model is imposed by using actual meteorological data and river discharge data. At the sea side open boundary, the water level is specified with the real time series of observed data. The fresh water discharge from five sources is included, being the total of the rivers Zenne, Dender, Nete and Durme, the river Scheldt, the docks of Antwerpen, the "Spuikanaal van Bath" and the "Kanaal van Terneuzen". The fresh water discharge is taken from ten-day averaged data.

At the sources the discharged water is completely fresh. At the sea side open boundary, the salinity is specified according to measurements and data taken from a North Sea model.

The hourly varying wind speed and - direction is also taken from measured data. The local effect of wind is not very important, but the wind induced water elevation variation in open boundary can influence the water movement and salinity distribution in the estuary significantly.

2.4 Initialization.

The flushing time of the Scheldt estuary is in the order of a few months. In order to decrease the initialization time, we used an averaged salinity distribution which corresponded tot the actual discharge conditions. It is expected that the simulation period is long enough for salinity to reach a dynamic equilibrium with this initial condition. This is not verified however. To check this assumption, we should shift the starting time of simulation period several days backwards and then compare the results with the previous results. This should be done in future.

3.0 Period over which the simulations took place.

The model simulations started at March 20 1989 and lasted for 24 days until April 13 1989. This period was chosen such that a number of measured time series for waterlevels, salinity and velocity were available. The latter parameter should have been registered at a number of vertical positions in the watercolumn. An extra demand was the presence of field data concerning suspended sediment at a number of locations in the estuary. This put some restrictions to the choice of the simulation period.

3.0.1 Observed waterlevel timeseries.

For calibration, water level measurements are collected in 7 stations, Vlissingen, Terneuzen, Hansweert, Baalhoek, Bath, Prosperpolder and Antwerpen.

3.0.2 Observed velocity timeseries

In the modelling period, four measurement campaigns were undertaken over a cross section in the Westernscheldt. On April 4, eight vessels were used to

cover the cross section "Nauw van Bath / Schaar van de Noord". Current velocities were measured at a number of depths during 13 hours. On April 12 the same transect was monitored once more. Unfortunately, for April 12 the digital data at some stations was lost and for these stations only depth averaged data is available.
On April 6 current velocities were measured during 13 hours near Terneuzen. At four locations along the cross section data is available at a number of depths.
Finally on April 10 current velocities were measured again during 13 hours at a transect near Breskens. For this period at five locations along the section data is available at different depths. During all campaigns also suspended sediment concentration was measured.

In figure **3** the locations of the vessels during the measurements is given. In table **3-0** the corresponding names are given.

Table 3-0: Names and locations of vessels corresponding to figure **3**.

Date	Name of vessel	Location number (fig 3)
April 4	Swalinge	1
	Steenvliet	2
	Wijtvliet	3
	Pluimpot	4
April 6	Wijtvliet	1
	Steenvliet	2
	Swalinge	3
	Pluimpot	4
April 10	Pluimpot	1
	Swalinge	2
	Steenvliet	3
	Molenvliet	4
	Wijtvliet	5
April 12	Steenvliet	2
	Swalinge	5

3.0.3 Observed salinity data.

Long-term salinity measurements are available at 4 station, Hoofdplaat, Baalhoek, Prosperpolder and Oosterweel. At April 10, there is an excursion was undertaken from Vlissingen to Temse (upstream from Antwerpen) to take water samples in 7 station. At every station 1 sample was taken at the surface. This cruise gives us useful information about the salinity gradient in the estuary.

3.1 Calibration and validation of the model

3.1.1 Waterlevels

In 7 stations, simulated water level is compared with the observations. The agreement between the calculations and the observations is quite well (figures **4.1-7**). The comparisons of high water level, low water level, flood and ebb duration are listed in table **3-1** and table **3-2**.
It is not surprising that in Vlissingen and Terneuzen the difference between simulation and observation is not significant, for the observations at these two station are used as a boundary condition for the numerical model. Further upstream, the model result show some deviation from the observations. In Properpolder, the difference between simulated low water level and observed low water level reaches 0.15*m*, relative error is about 6%.

Table 3-1. Comparison of simulated and observed high and low water levels (April 12).

Location		Vlissingen	Terneuzen	Hansweert	Baalhoek	Bath	Prosper-polder	Antwerpen
Low Water (*m*)	Simulation	-2.12	-2.28	-2.38	-2.43	-2.44	-2.49	-2.63
	Observation	-2.15	-2.27	-2.37	-2.44	-2.45	-2.51	-2.65
	Error	0.03	-0.01	-0.01	0.01	0.01	0.02	0.02
High Water (*m*)	Simulation	1.78	2.05	2.28	2.44	2.59	2.66	2.76
	Observation	1.79	2.01	2.23	2.43	2.50	2.50	2.73
	Error	-0.01	0.04	0.05	0.01	0.09	0.15	0.03
Low Water (*m*)	Simulation	-1.62	-1.75	-1.86	-1.92	-1.93	-1.97	-2.13
	Observation	-1.65	-1.78	-1.90	-1.96	-2.01	-2.01	-2.14
	Error	0.03	0.03	0.04	0.04	0.08	0.04	0.01
High Water (*m*)	Simulation	1.80	2.07	2.29	2.45	2.59	2.66	2.80
	Observation	1.82	2.06	2.24	2.45	2.51	2.51	2.79
	Error	-0.02	0.01	0.05	0.00	0.08	0.15	0.08

Upstream from Hansweert, the simulated flood duration is shorter and simulated ebb duration is longer than observed. This suggests that the nonlinear effect is a little over estimated. The error may origin from following aspects:

- Bottom friction and turbulent nonlinearity.
- The flooding and drying of tidal flats. Both spatial resolution and the methodology of wet-dry judgement can yield errors. It has been pointed out that the simulated flooding and drying processes are always later in phase than actual processes.
- Topography in the model. The 400 meter resolution is not fine enough to represent the narrow water channels. This may influence the shallow water nonlinearity.

If the simulated results and observed results were harmonically analyzed and compared afterwards, it would be possible to find out which of the previously mentioned items is the most important source for errors. The shallow water nonlinearity which generates even multiples of M_2, or the bottom friction (which depends quadratically on the bottom velocity) and Prandtl's mixing length turbulent model which generate odd multiples of M_2.
In most case the error of flooding and ebb duration in the simulations is about 6-7%, only in Antwerpen it can reach higher values (table **3-2**).

Table 3-2. Comparison of simulated and observed flooding and ebb duration (April 12).

Location		Vlissingen	Terneuzen	Hansweert	Baalhoek	Bath	Prosper-polder	Antwerpen
Flood Duration (*Hours*)	Simulation	5.58	5.41	5.50	5.53	5.16	5.09	4.74
	Observation	5.65	5.61	5.76	5.69	5.48	5.48	5.32
	Error	1%	4%	5%	3%	6%	7%	11%
Ebb Duration (*Hours*)	Simulation	6.59	6.67	6.59	6.53	6.84	6.83	7.13
	Observation	6.75	6.62	6.30	6.26	6.50	6.50	6.72
	Error	2%	1%	5%	4%	5%	5%	6%
Flood Duration (*Hours*)	Simulation	6.00	5.84	5.92	5.93	5.69	5.67	5.35
	Observation	5.75	5.80	6.08	6.16	6.00	5.99	5.66
	Error	4%	1%	3%	4%	5%	5%	6%

3.1.2 Current velocity.

The exact location at which the measurements took place is generally not present as a grid point in the model. Besides, the location of the measurement vessels was known with some uncertainty.
In order to obtain information from the observation at grid points of the model, the simulated current velocities were interpolated to the location of the measurement. This turned out to be a rather tricky business, as the current field showed strong spatial variation even at the scale of the model grid. A bilinear interpolation did not always turn out to be sufficiently accurate.

In figures **5.1-4**, the simulated surface layer and bottom layer velocity is plotted together with depth averaged observed velocity for four stations in the transect on April 12. Among them are station 5 and 6 from tabel **3-0**. In table **3-3** some characteristic aspects of the observed and simulated current velocities are compared.

The general shape of calculated curves is similar to the observed current timeseries. The simulated maximum velocity shows some deviation from the observed maxima. One explanation is the sensitivity of the current data to local topography. From a bathometry chart with a fine resolution, we can clearly distinguish two channels perpendicular to the measurement transect. Both channels are deeper that 15*m*. Between the channels there is a bank where the waterdepth is less. The width of the channels and the width of the shallow bank is less than 400*m*. So this topographic feature can not be resolved in the 400*m* modelgrid we are using. Unresolved topographic features can be the cause for some of the deviations between observed data and model results.
The characteristics of currents in the two channels differs much. In the northern channel the ebb current dominates, while in southern channel the flood current dominates. From observation we know that the gradient of the current in this region can become quite large.

Apart from the depth averaged current data vertical current profiles were available at a number of locations over different periods (see *3.0.2*).
In figures **6.1-12** the model results are plotted together with the measurements at the surface as well as at the bottom. There's generally good agreement between the data and the model, not only for April 12, but also for the other days. The variation in time is quite reasonable, the bottom velocities calculated

by the model are a little lower than could be expected from the data.
The parameters of the model were calibrated on the April 12 data. The data availabe on the other days in April could be used for a first validation of the model.

We have to conclude that the spatial resolution used can resolve the general current structure, but does not always give the details in the current field which are present in the observations and are caused by the fine scale topographic features. The use of a modelgrid with a higher resolution would probably solve this problem. Nevertheless, the results given by the 400*m* grid seem to be a good starting point.

Finally we show the current field during a tidal cycle at the surface as well as at the bottom in figure **7.1-4**. The period covered is from just after high water till high water with an interval of one hour. Ebb-dominated and flood-dominated channels are clearly visible. Comparison of the velocity fields at 11.00 and 18.00 at the surface, shows clear ebb-dominance in the "Zuidergat channel" and flood-dominance in the "Schaar van Valkenisse". A view of ebb - and flood dominance over the whole estuary calculated by the model is presented in figure **8**.
In figure **9** (near Bath) it is shown that the turn of the tide at low water at the bottom precedes the turn at the surface.

Table 3-3. Comparison of maximum flood and ebb current at the surface and near the bottom on April 12.

Location			Pluimpot	Wijtvliet	Zeekat	Steenvliet	Swalinge
Maximum Flood Velocity (*m/s*)	Surface	Simulation	0.55	0.74	1.11	1.21	1.46
		Observation	0.71	1.56		1.54	1.14
		Error	-0.16	-0.82		-0.33	0.32
	Bottom	Simulation	0.48	0.64	0.79	0.79	1.06
		Observation	0.50			1.00	1.00
		Error	-0.02			-0.21	0.06
Maximum Ebb Velocity (*m/s*)	Surface	Simulation	1.24	1.15	0.73	0.55	1.14
		Observation	1.46	1.41	0.61	0.75	1.45
		Error	-0.22	-0.26	0.12	-0.20	-0.31
	Bottom	Simulation	0.64	0.75	0.53	0.38	0.79
		Observation	0.80	1.00	0.41	0.31	1.19
		Error	-0.16	-0.25	0.12	0.09	-0.40

3.1.3 Salinity.

Long-term salinity measurements are available at 4 station, Hoofdplaat, Baalhoek, Prosperpolder and Oosterweel. The comparison of simulated surface salinity and the observed surface salinity is shown in figure **10.1-2**. The simulation and observations agree quite well. In Prosperpolder, the result is nearly perfect. Maximum absolute error is only 2‰.
On April 10, there has been an excursion from Vlissingen to Temse (upstream from Antwerpen) and water samples were taken at 7 station. At every station 1 sample was taken. The simulated and observed salinities are listed in table **3-4**. The maximum

absolute error is 1.3‰. In figure **11** the observed data are plotted against the simulated salinity. The drawn line indicates the perfect agreement.
The simulated salinity distribution, especially the gradient, is quite satisfactory. This latter point is important in view of the role the salinity distribution plays in the 3D structure of the current field. Near the location of the maximum salinity gradient, this should lead to a density driven bottom current which is oppositely directed to the surface current. High concentrations in suspended sediment (turbidity maximum) are located near the maximum salinity gradient. This is an important phenomenon for sediment transport.

In figure **12.1-2** the evolution of the salinity field in time is shown in the bottom layer and at the surface. Starting at high water, the salinity field is shown every hour. At high water the watercolumn stratifies due to tidal adjustment. From low water to high water, the relatively salt water is pushed upstream. At high water a strong horizontal density gradient is present near the Dutch-Belgian border. At the turn of tides the stronger tidal currents at the surface tilt the horizontal density gradient and stratified conditions exist in a limited area over a short period (somewhat more than an hour). This phenomenon does not appear at the turn of tides after low water. In this case the horizontal density gradient is weaker and the instable watercolumn (reversed stratification) is mixed up rappidly.

Table 3-4. Comparison of simulated salinity and observed salinity data.

Location	Simulation	Observation	Absolute Error
Vlissingen	28.64	28.85	-0.21
Honte	27.64	26.85	0.79
Terneuzen	24.06	23.35	0.71
Zuidergat	16.10	14.80	1.30
Lamswaarde	12.64	11.65	0.99
Bath	8.77	8.45	0.32
Schaar van Ouden Doel	4.56	4.08	0.48

3.2 Residual velocity.

To get a first impression of the transport over a tidal cycle the residual tidal velocity is often used. This not completely correct, as the averaging of the velocity takes place at a fixed location in space (Eulerian), while the transport of water or sediment is determined by the velocities along the transport path (Lagrangian). Nevertheless, the residual velocity field can give us some information about the curent structure. In figure **13.1** the residual velocity at the surface and at the bottom in the region near the turbidity maximum is shown. Counteracting surface - and bottom currents can be observed in the area where the river tail emerges (figure **13.1**). The structure of ebb - and flood dominated channels also becomes visible from the inspection of the residual current structure and agrees with the results given in figure **13.2** (figure **8**).

4.0 Some sensitivity analysis.

4.0.1 Influence of the factor C_μ in the turbulence model on the vertical velocity profile.

The vertical structure of the current velocity, is very sensitive to the factor on parabolic

vertical eddy viscosity (table **3-5**). The recommended (default) value 0.55 yields a too small difference between the surface - and bottom velocity. After some numerical experiments, the factor on parabolic vertical eddy viscosity is specified as 0.20

Table 3-5. Influence of the factor on parabolic vertical eddy viscosity on the vertical current structure for the April 12 data.

Location	Max surface ebb velocity		Max bottom ebb velocity		Difference	
	C_μ=0.55	C_μ=0.20	C_μ=0.55	C_μ=0.20	C_μ=0.55	C_μ=0.20
Pluimpot	0.95	1.22	0.73	0.60	0.23	0.62
Wijtvliet	0.90	1.01	0.75	0.73	0.15	0.28
Zeekat	0.55	0.59	0.40	0.37	0.15	0.22
Swalinge	0.94	1.11	0.65	0.79	0.29	0.32

The factor on parabolic vertical eddy viscosity also influences water elevation. Decreasing the value of the factor will increase flooding duration and decrease ebb duration. This is due to the fact that decreasing the factor C_μ will decrease turbulent nonlinearity.

4.0.2 The influence of the Manning coefficient in the bedstress formulation.

The Manning coefficient has certain influence on current vertical structure. Decreasing the Manning coefficient will decrease the bottom friction, and hence the bottom velocities will increase slightly. The tidal elevation upstream is quite sensitive to the bottom friction parameter. The tidal difference will increase when the Manning coefficient is decreased.
The value of the Manning coefficient also influences the vertical shear in the velocity field, and indirectly has an influence on the salinity distribution.

5.0 Overall view of the model results.

The results of the model are satisfactory for our purposes. The behaviour of the waterlevels generated by the model is in agreement with the results that are shown in [Lievense, 1994]. At the seaward boundary very good agreement with reality is observed. Upstream from Bath deviations up to 0.15*m* between observed and simulated waterlevel can occur (Prosperpolder). Over the whole model area the duration of the flood period is overestimated and the ebb duration is underestimated compared to observations. Maximum deviations occur in the region near Antwerpen.
The evolution of the current velocities in time in generally in good agreement with observations. Surface currents however are somewhat underestimated by the model. Bottom current velocities are in line with reality. The vertical shear in the velocities profiles is generally a little too small. As we intend to use the model for sediment transport purposes, our main interest lies in good representation of the bottom current velocities. Small scale topographic features can have a strong local influence on the current profiles.
The representation of the salinity field by the model is very good, almost perfect in line with observations. The representation of the horizontal salinity gradient by the model is important with respect to the position of the turbidity maximum in the estuary. A density driven secundary current is observed near the location of the maximum salinity gradient. Stratification caused by tidal adjustment is represented.

Appendix A

Vertical turbulent mixing

Horizontal turbulent transports of momentum and salinity are represented by viscosity and diffusion terms in the equations for momentum and salinity.
The vertical coefficients for turbulent exchange of momentum and salinity depend on a vertical mixing length scale L, the turbulent kinetic energy, on vertical velocity shear and on functions of the gradient Richardson number Ri.

Turbulent kinetic energy K is modelled algebraically using a mixing length (L) approach. The equations for the vertical turbulent viscosity ν_z(K,L) and vertical turbulent diffusion $D_z(\nu_z)$ then read:

$$\nu_z = c_\mu L\sqrt{K}$$

with c_μ a constant, and

$$D_z = \frac{\nu_z}{\sigma_z}$$

σ_z the Prandtl-Schmidt number which relates viscosity to diffusion.

For L the so-called Bakhmetev profile was assumed:

$$L = \kappa(z+d)\sqrt{1-\frac{z+d}{H}}$$

with z = -d the bottom and z = ζ the surface and H the total water depth, and K is modelled as:

$$K = \frac{1}{\sqrt{c_\mu}}\left(1-\frac{z+d}{H}\right)(U_{*b})^2 + \frac{1}{\sqrt{c_\mu}}\left(\frac{z+d}{H}\right)(U_{*0})^2$$

where U_{*b} the bottom shear stress and U_{*0} the surface shear stress

Turbulence is suppressed by stratification using Richardson number dependent damping functions. The first damping function F_L(Ri) acts upon the mixing length L:

$$FL(Ri) = \begin{cases} \exp(-2.3Ri) & Ri \geq 0 \\ (1-14Ri)^{0.25} & Ri < 0 \end{cases}$$

The second damping function F_σ(Ri) which acts upon the Prandtl-Schmidt number σ_z allows for extra damping on the vertical diffusion D_z:

$$F_\sigma(Ri) = \begin{cases} \dfrac{(1+3.33Ri)^{1.5}}{(1+10.0Ri)^{0.5}} & Ri \geq 0 \\ 1 & Ri < 0 \end{cases}$$

, i.e. the so-called Munk-Anderson approach.

For the 3D simulations we used the values c_μ = 0.20 and σ_z = 1.0 which gave good results.

Literature

Kuijper, E.V.L., (1993), Het 3D-KUSTSTROOK model gebaseerd op TRIWAQ-in-SIMONA, Rijkswaterstaat Dienst Getijdewateren, Report DGW-93.044.

Lander, J.W.M., Blokland, P.A. and J.M. de Kok (1996), The three dimensional shallow water model TRIWAQ with a flexible vertical grid definition, Rijkswaterstaat, National Institute for Coastal and Marine Management / RIKZ, Report RIKZ/OS-96.104X.

Llevense, P., (1994), Presentatie tweedimensionaal waterbewegingsmodel Scaldis400 van de Westerschelde en de Schelde, Rijkswaterstaat Zeeland Directorate, Report AX 94.072.

Figure 11: Measured versus modelled surface salinity at 7 locations in the Scheldt estuary.

Figure 12-1: Evolution of surface salinity on April 12 from 9.00 until 14.00.

Figure 12-2: Evolution of bottom salinity on April 12 from 9.00 until 14.00.

Figure 13-1: Eulerian residual circulation at the surface (top) and bottom (down) on April 12 near Bath.

Figure 13-2: Eulerian residual circulation at the surface (top) and bottom (down) on April 12 near Hansweert.

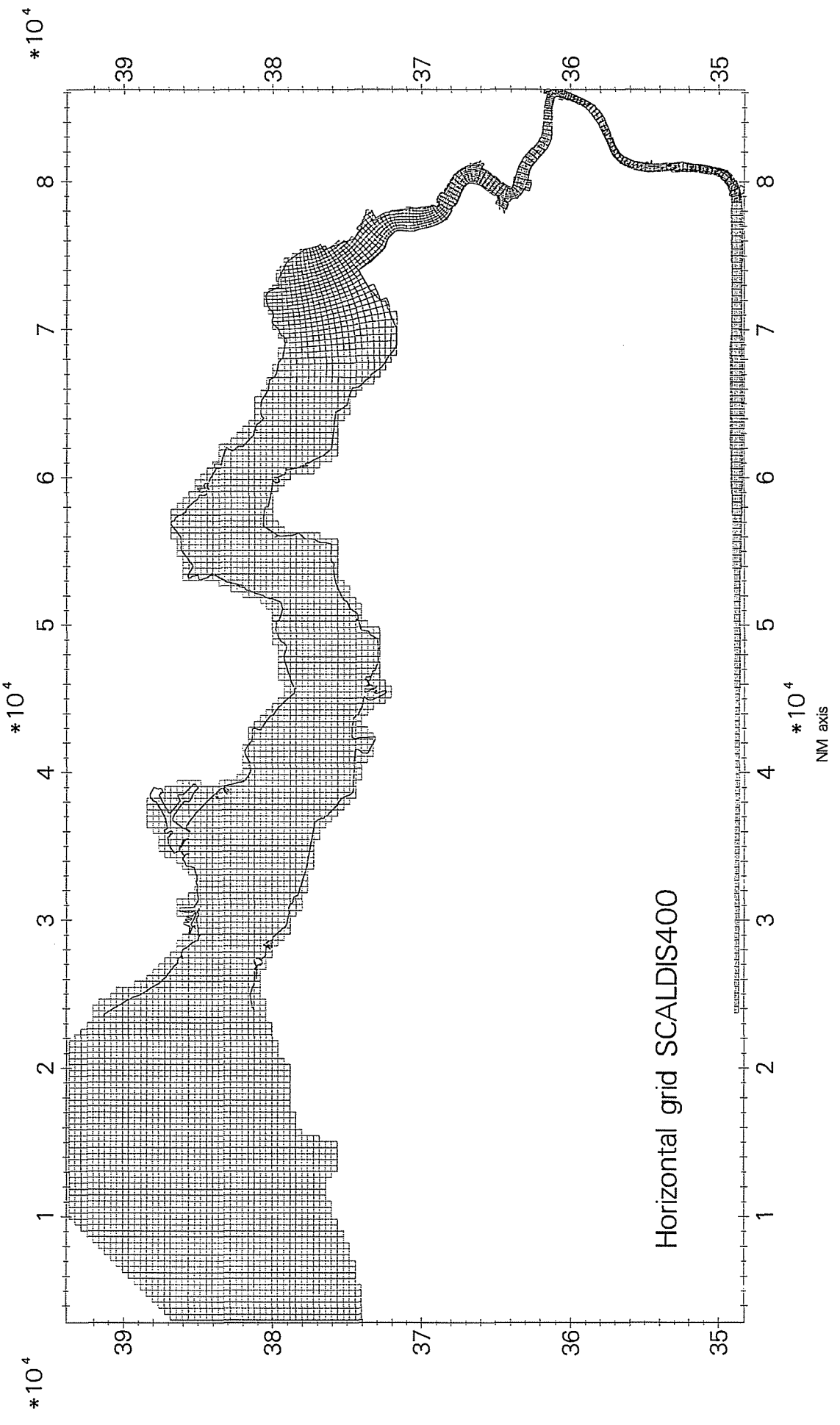

Figure 1: Horizontal grid Scaldis400 model.

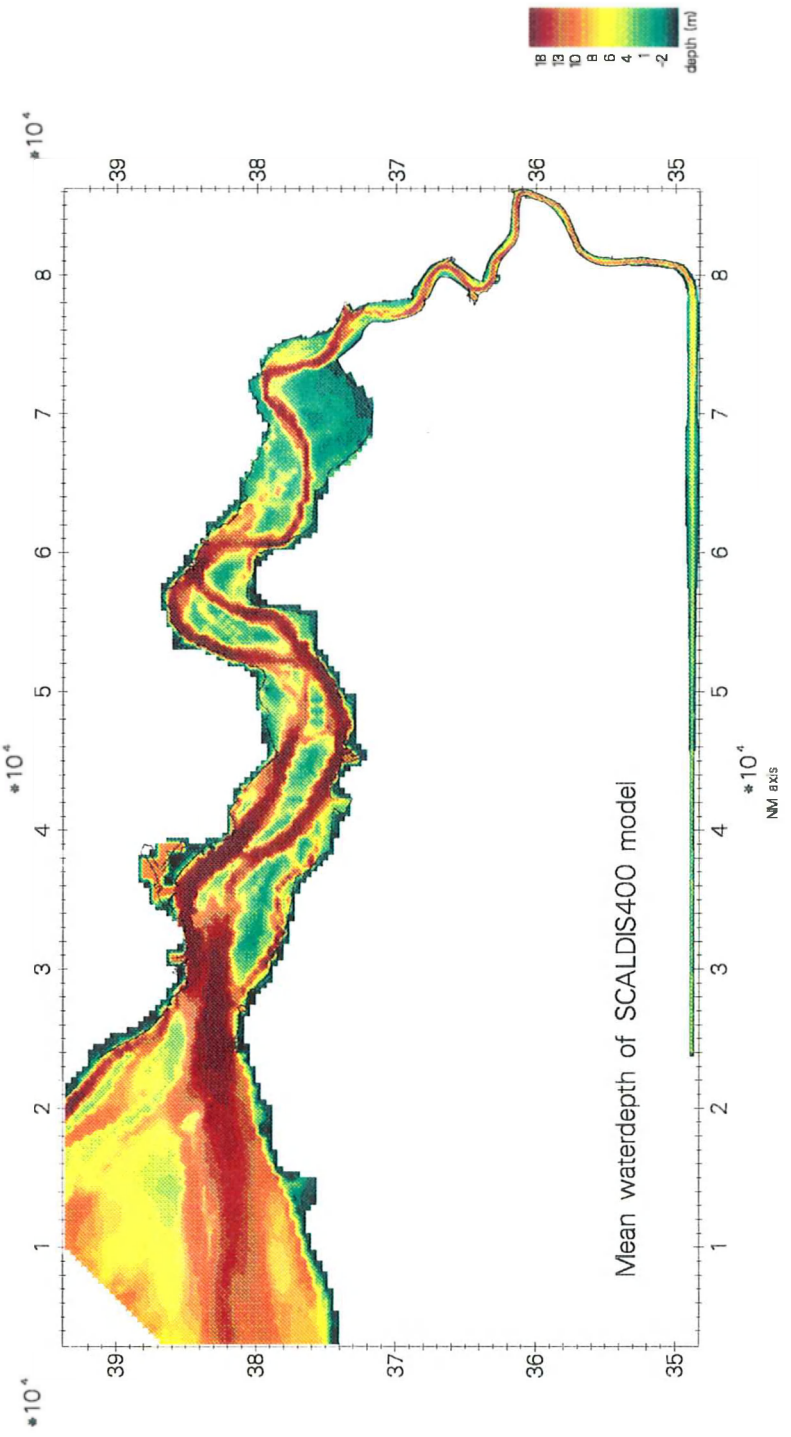

Figure 2: Depth chart of Scaldis400 model.

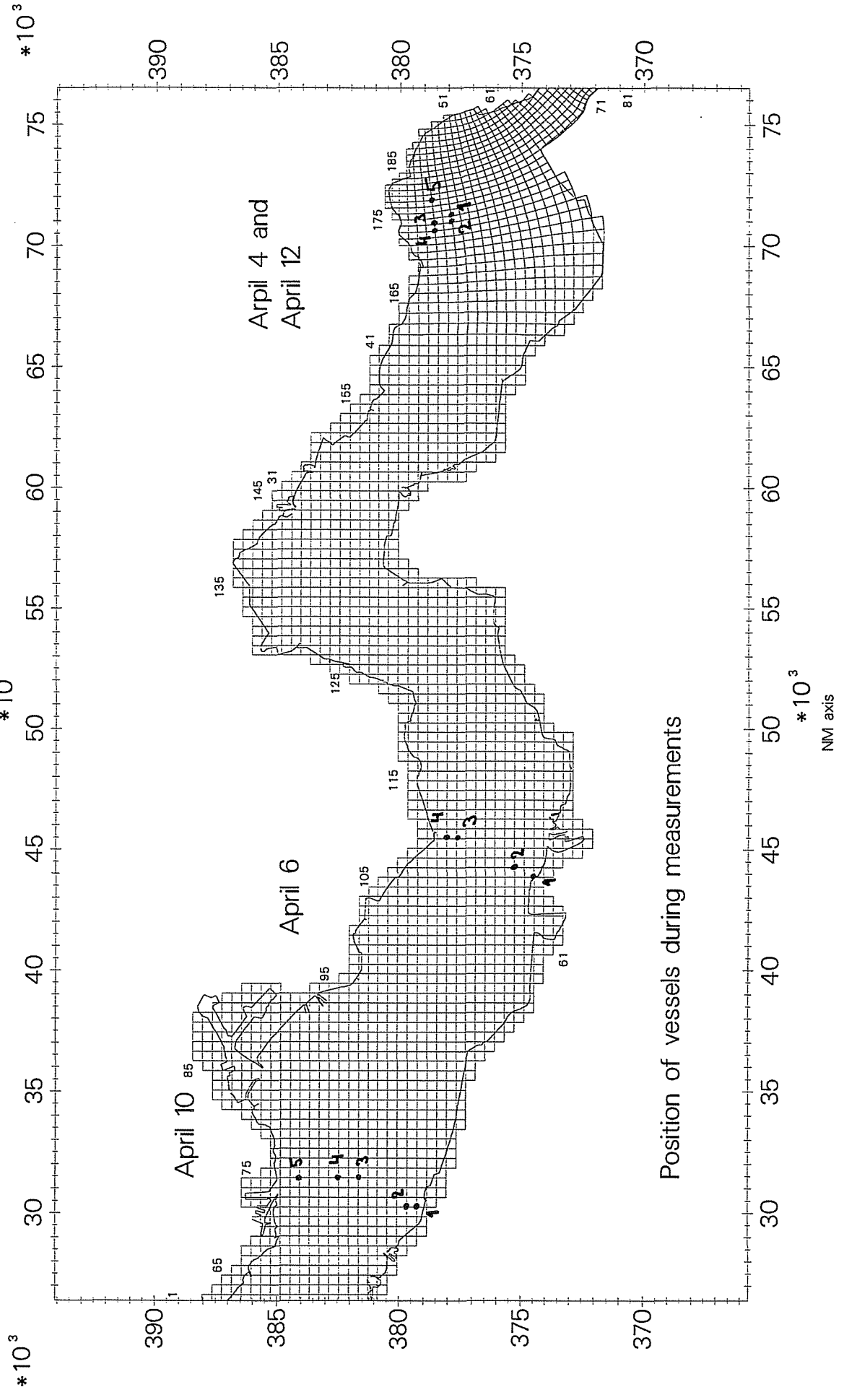

Figure 3: Locations of vessels during the measurements.

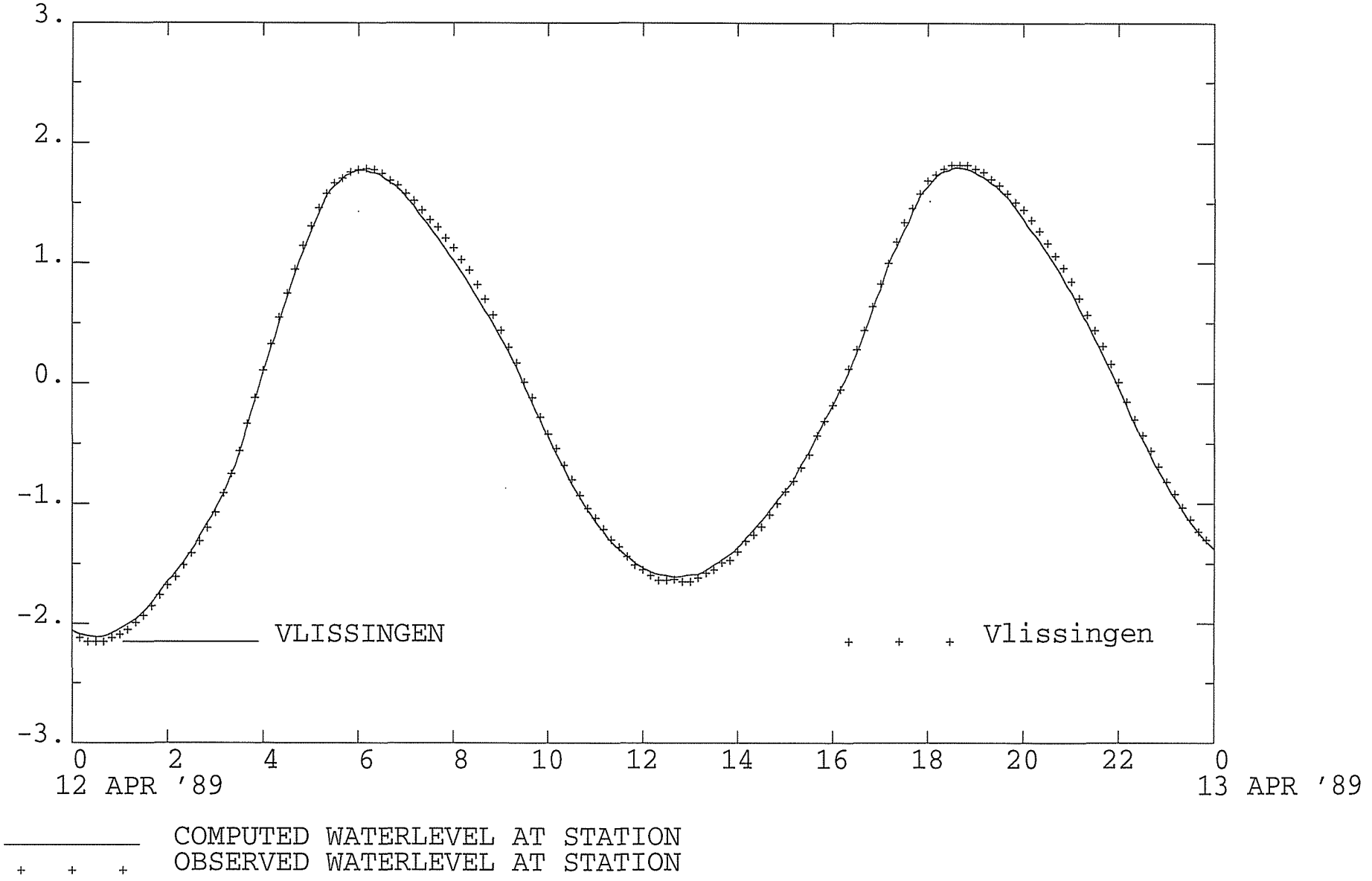

Figure 4-1: Waterlevel data versus model result at Vlissingen.

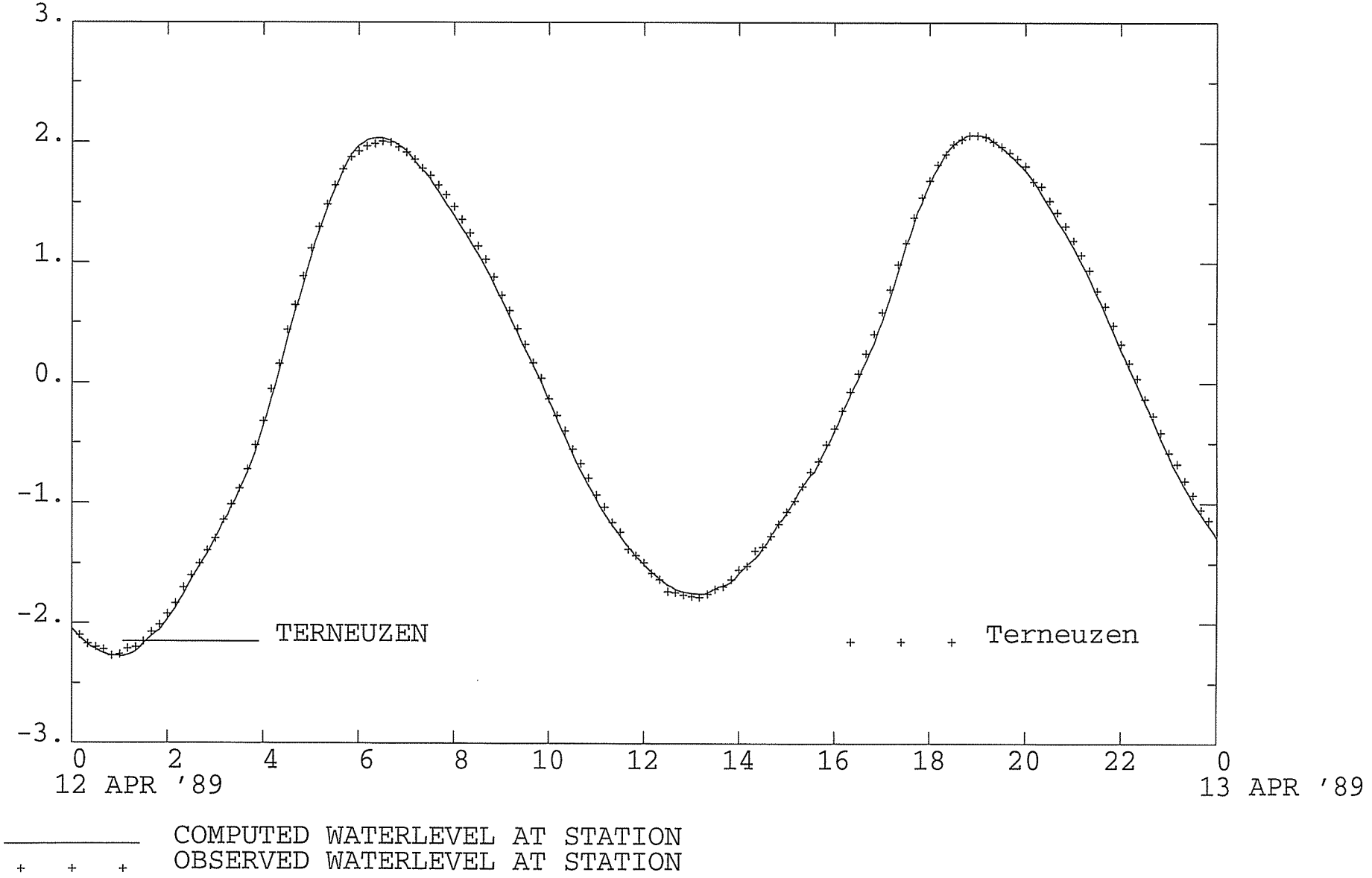

Figure 4-2: Waterlevel data versus model result at Terneuzen.

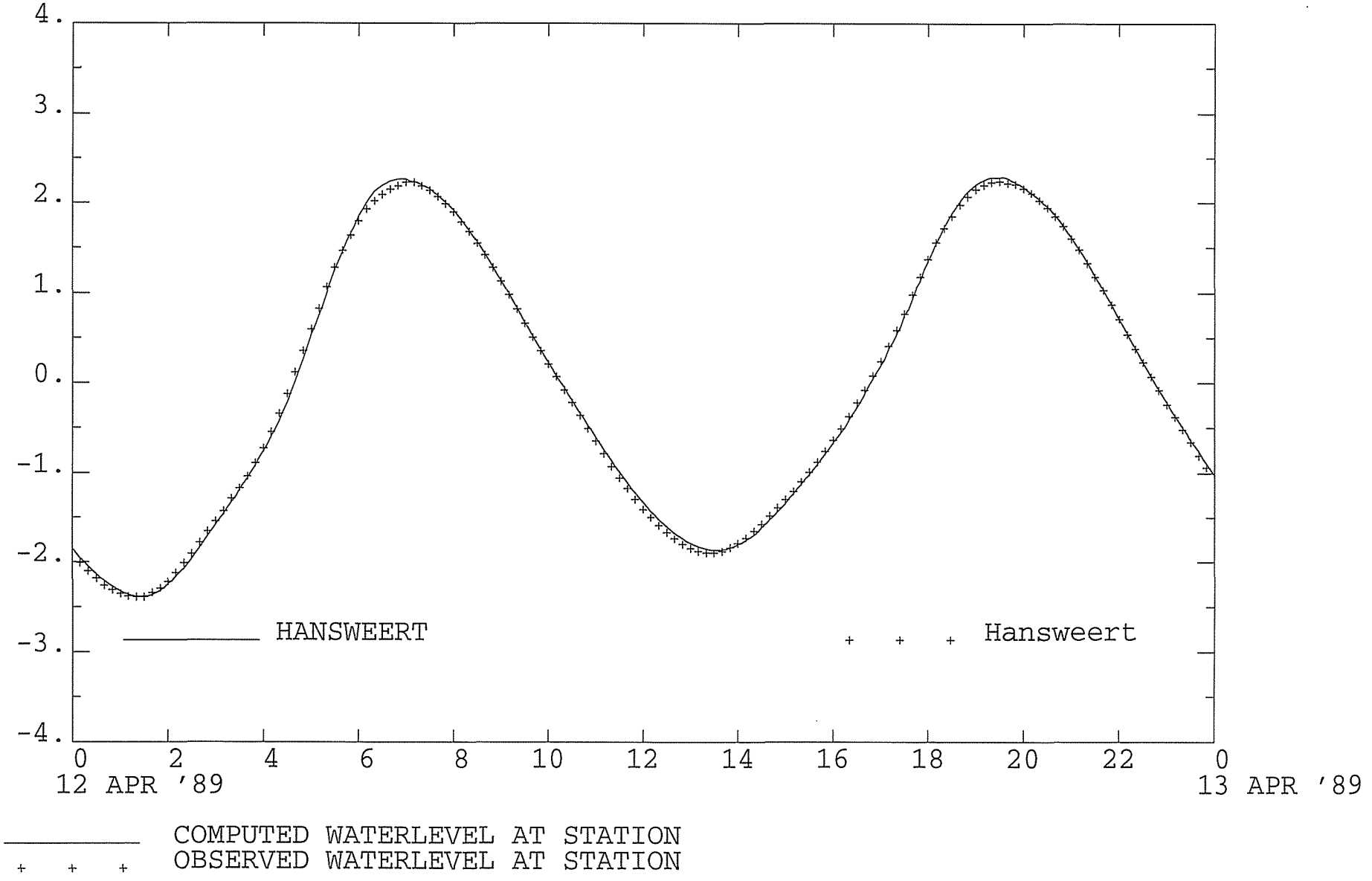

Figure 4-3: Waterlevel data versus model result at Hansweert.

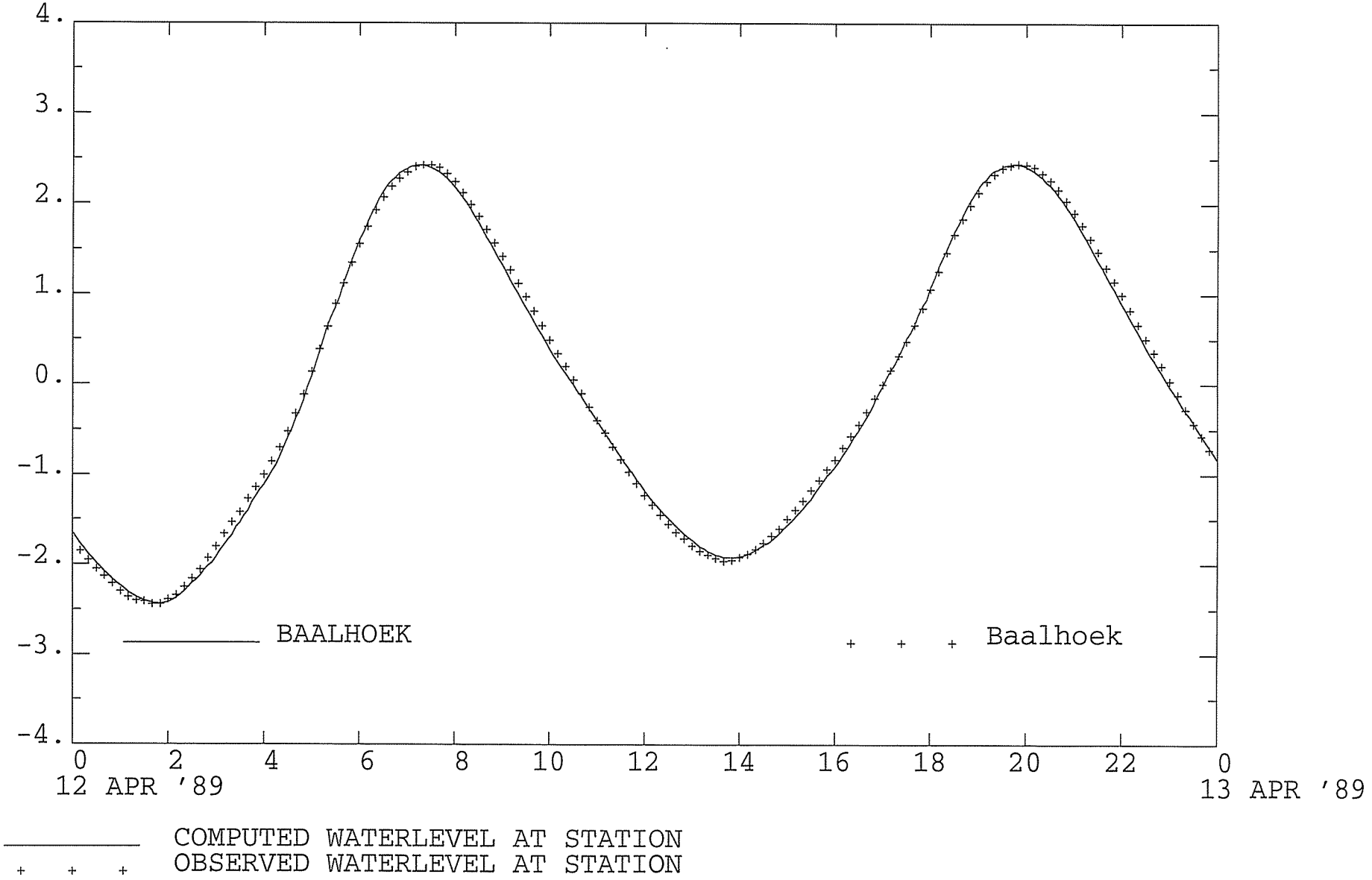

Figure 4-4: Waterlevel data versus model result at Baalhoek.

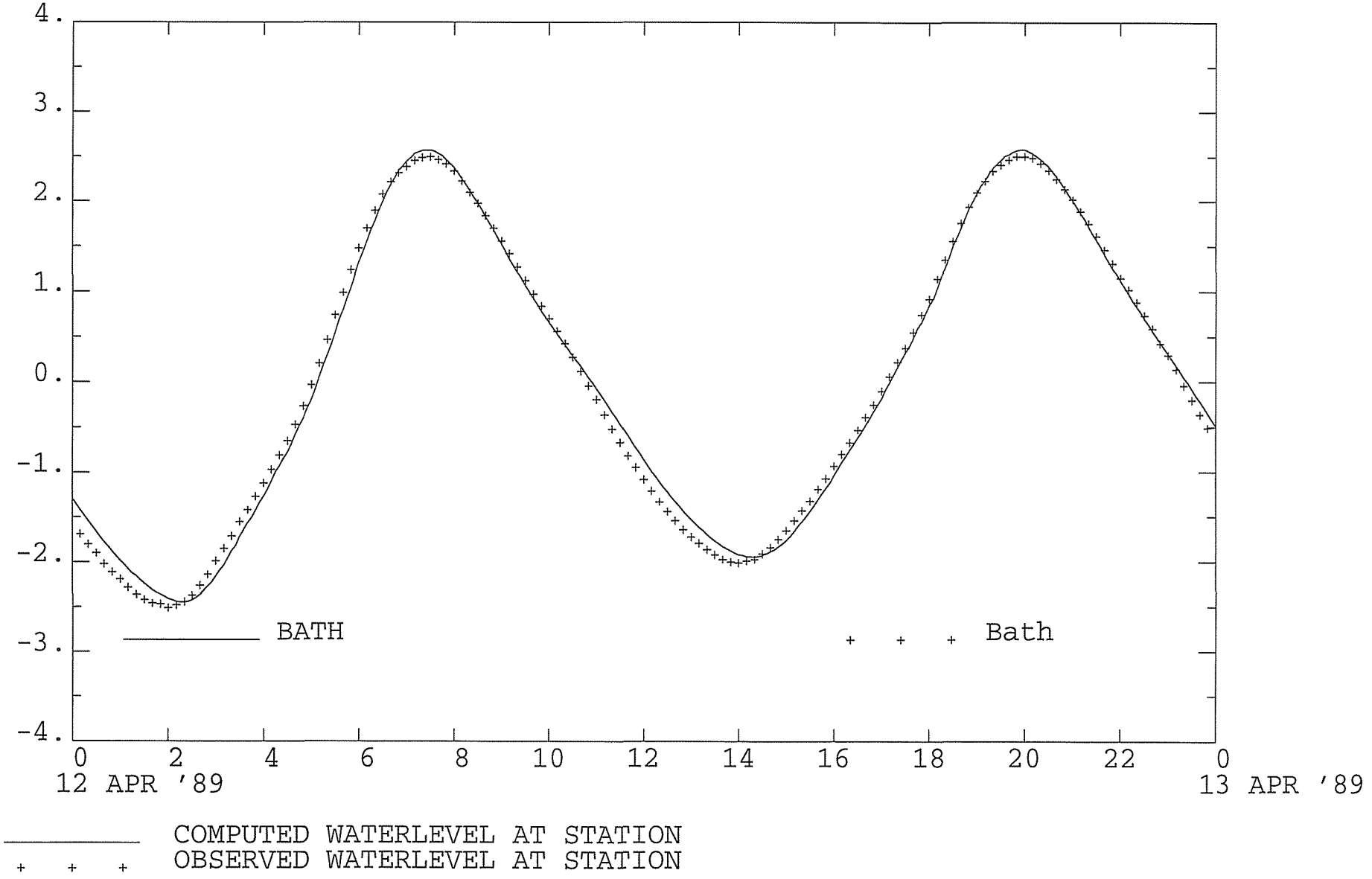

Figure 4-5: Waterlevel data versus model result at Bath.

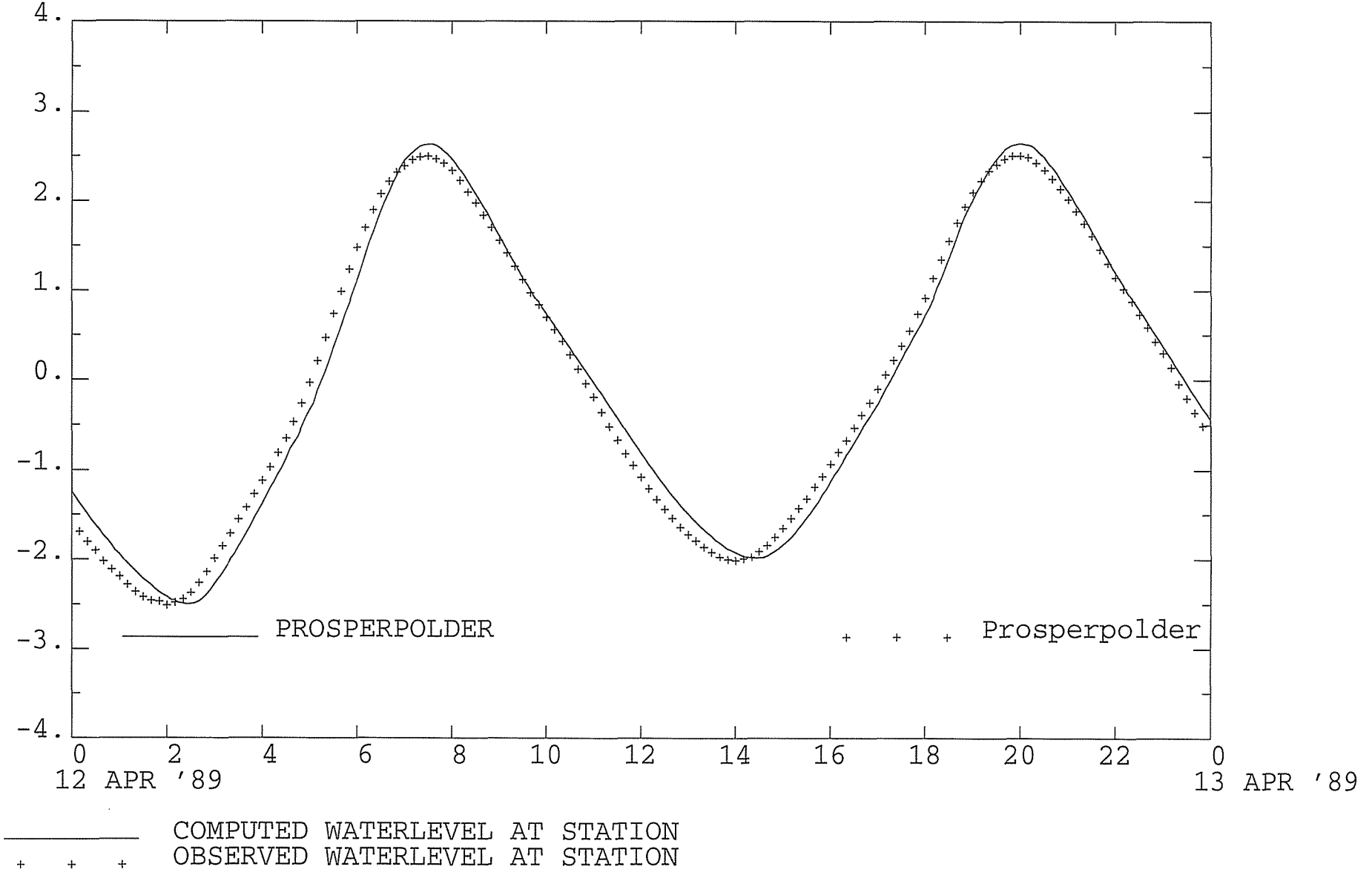

Figure 4-6: Waterlevel data versus model result at Prosperpolder.

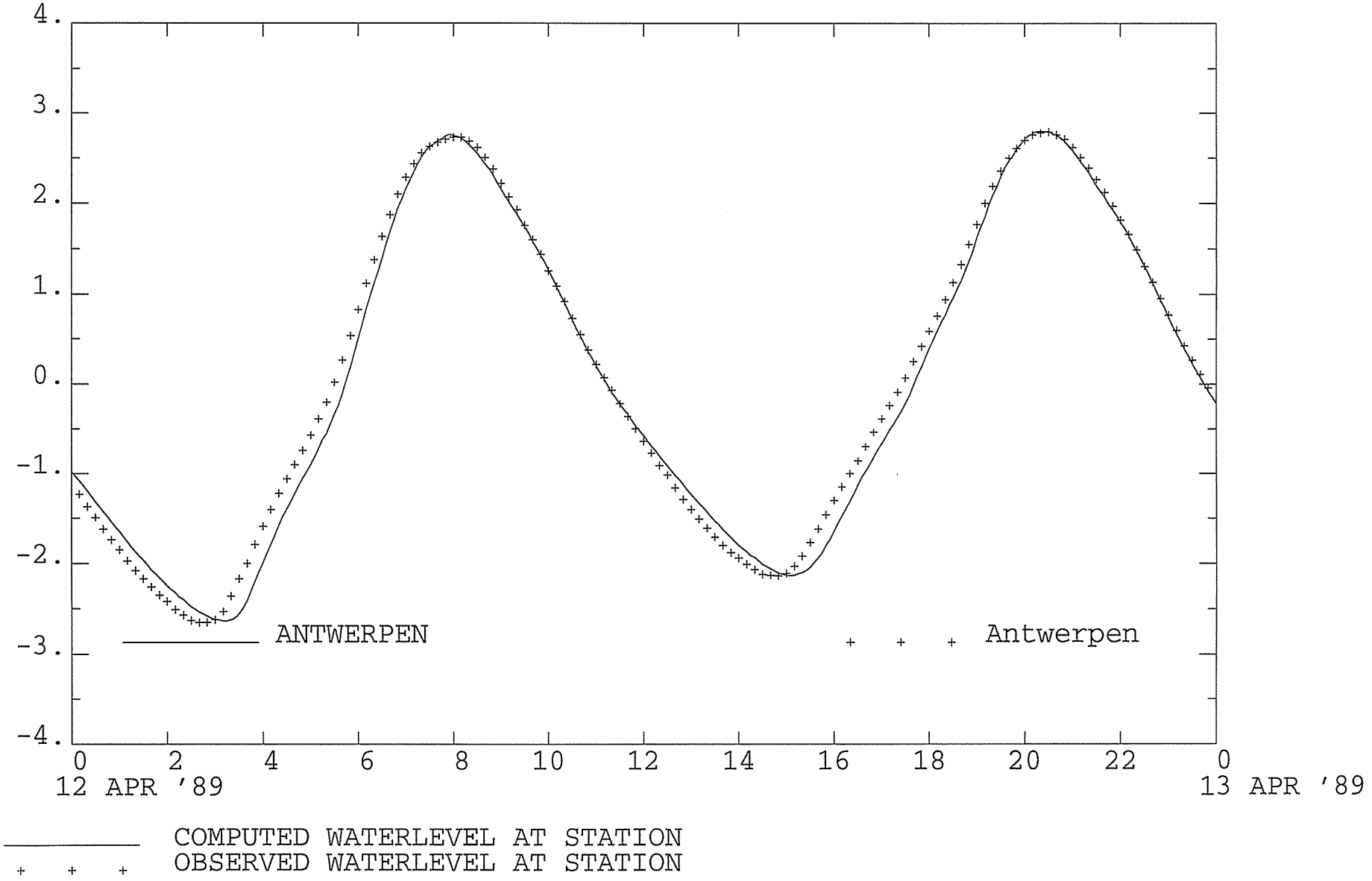

Figure 4-7: Waterlevel data versus model result at Antwerpen.

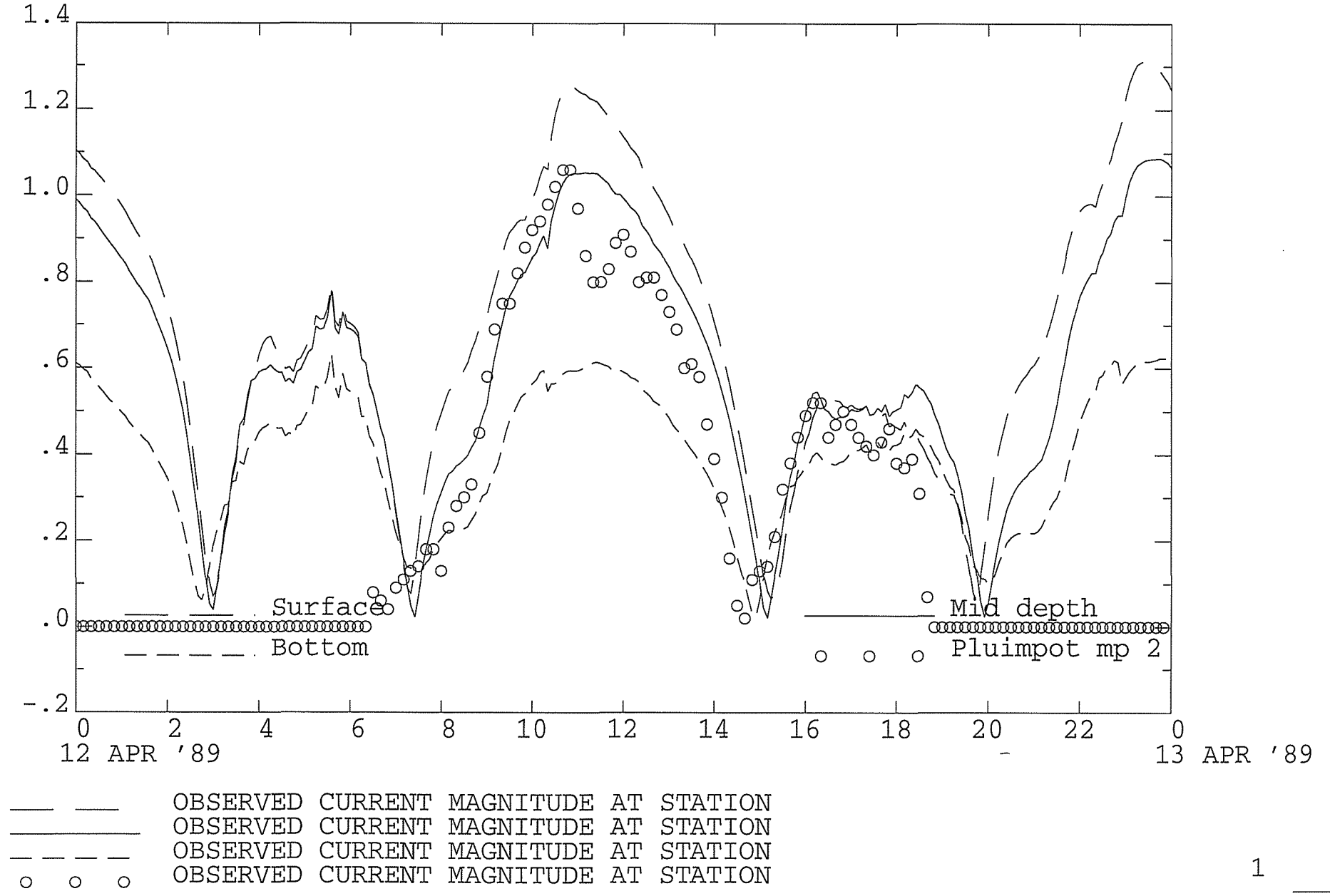

Figure 5-1: Depth averaged observed current velocity versus model result at various depths on April 12 at station Pluimpot.

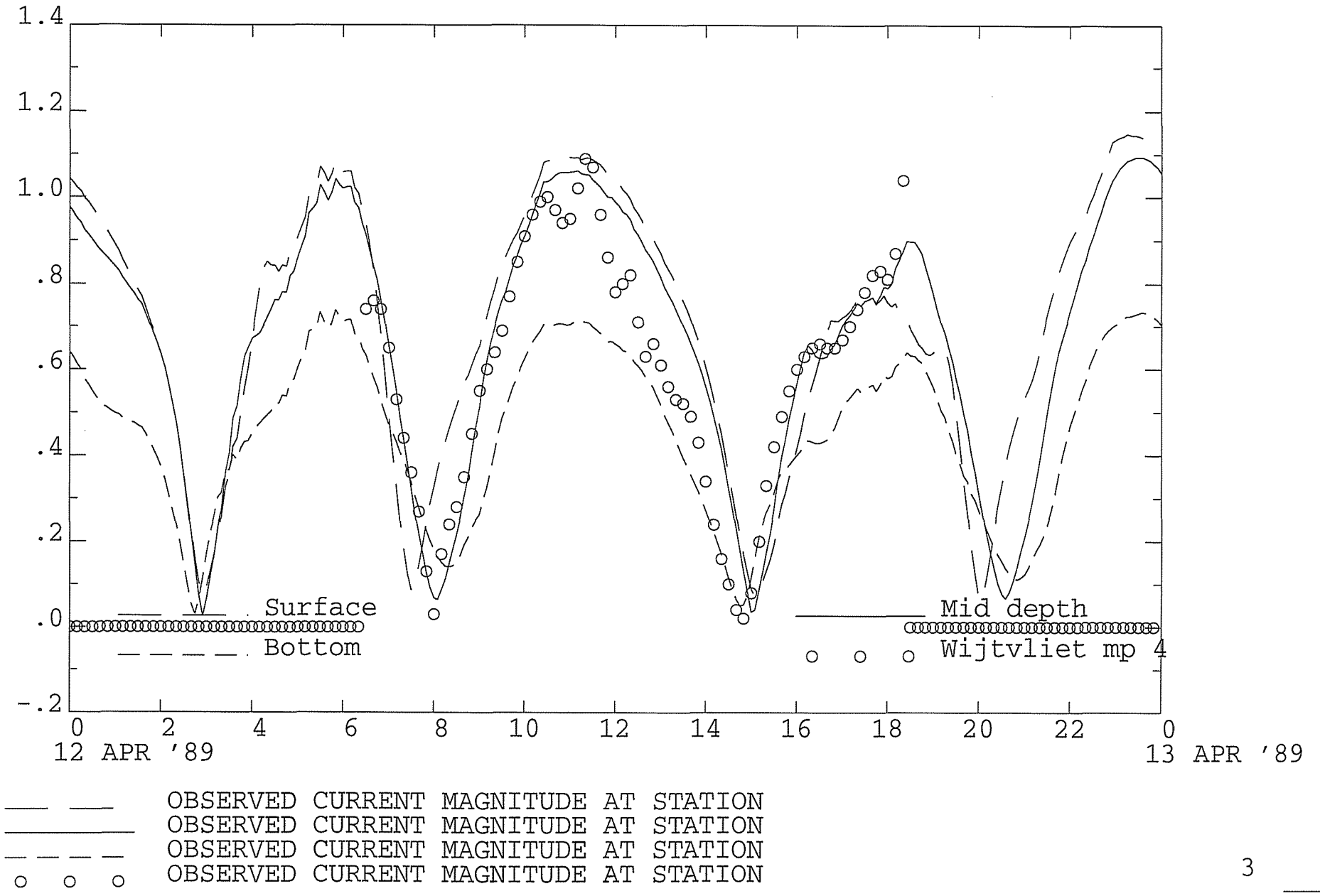

Figure 5-2: Depth averaged observed current velocity versus model result at various depths on April 12 at station Wijtvliet.

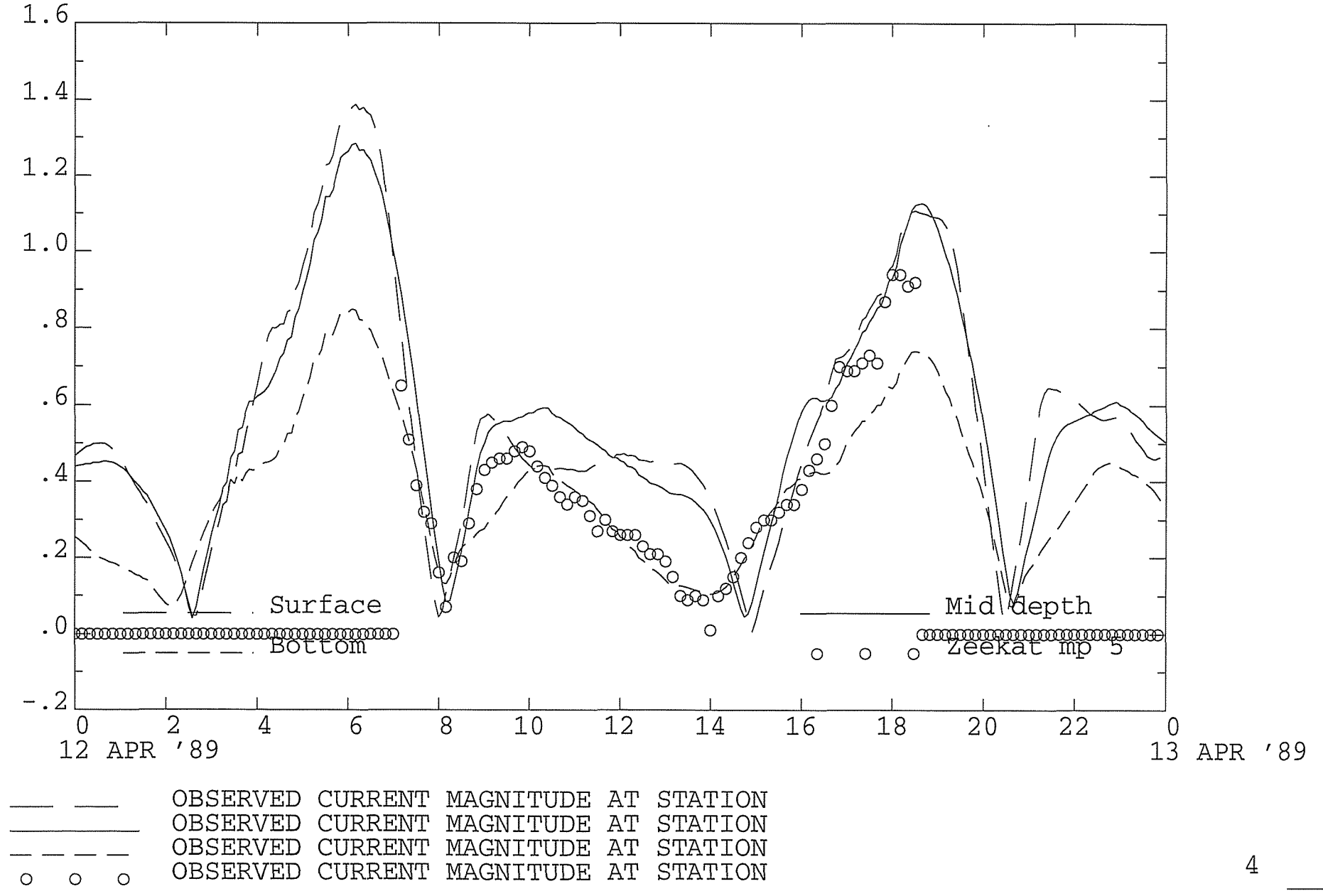

Figure 5-3: Depth averaged observed current velocity versus model result at various depths on April 12 at station Zeekat.

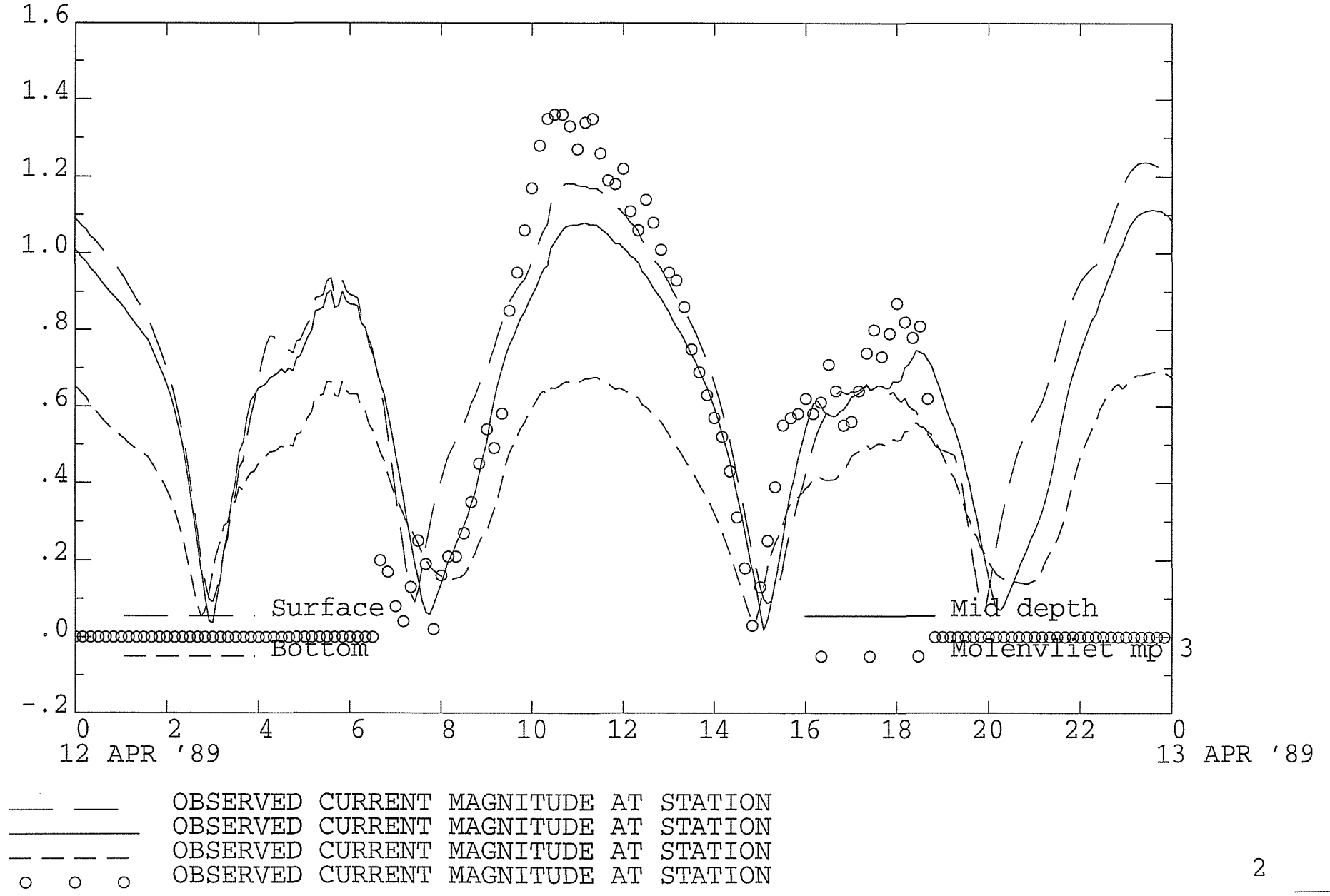

Figure 5-4: Depth averaged observed current velocity versus model result at various depths on April 12 at station Molenvliet.

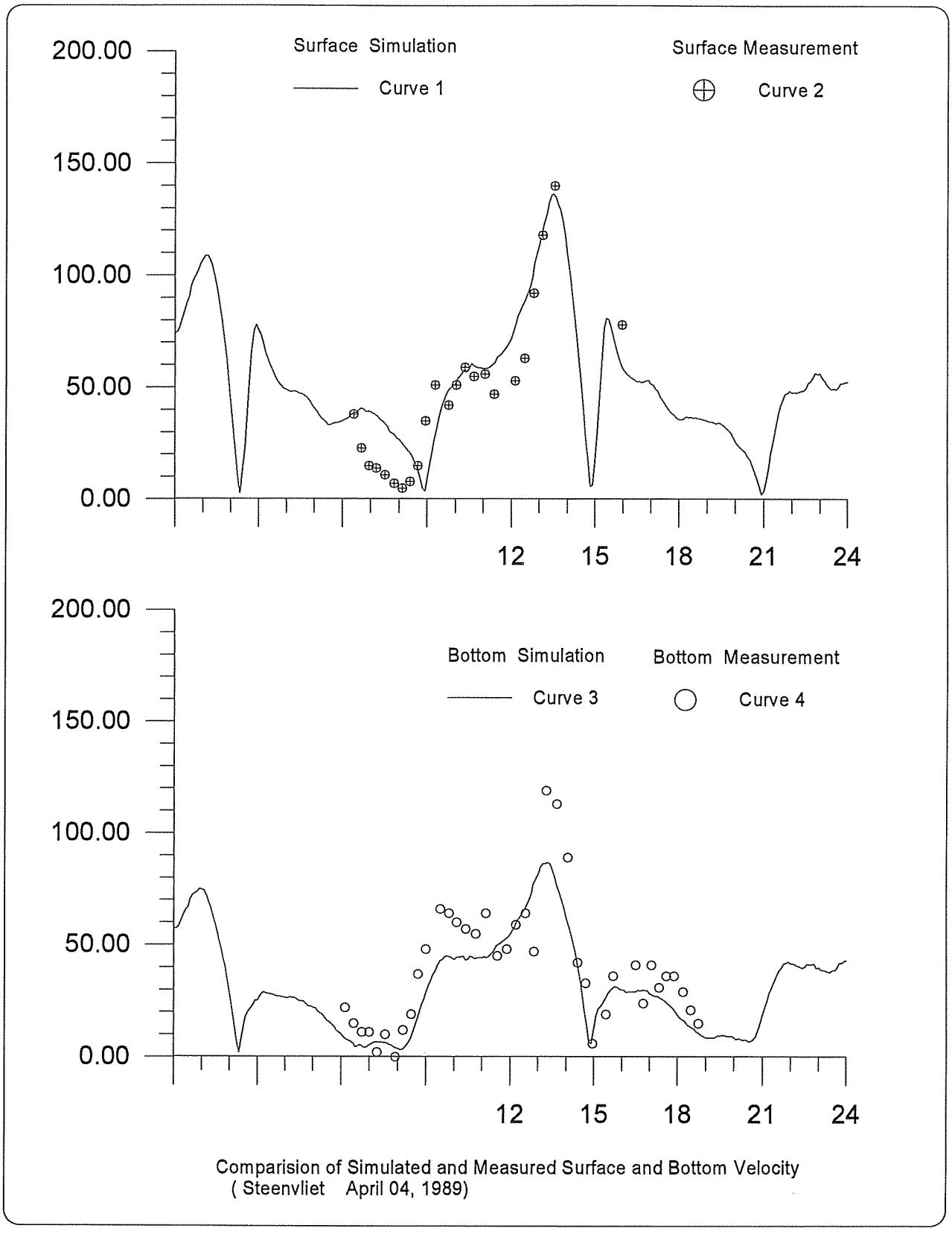

Figure 6-1: Comparison of simulated and measured surface and bottom current velocity on April 4 at station Steenvliet.

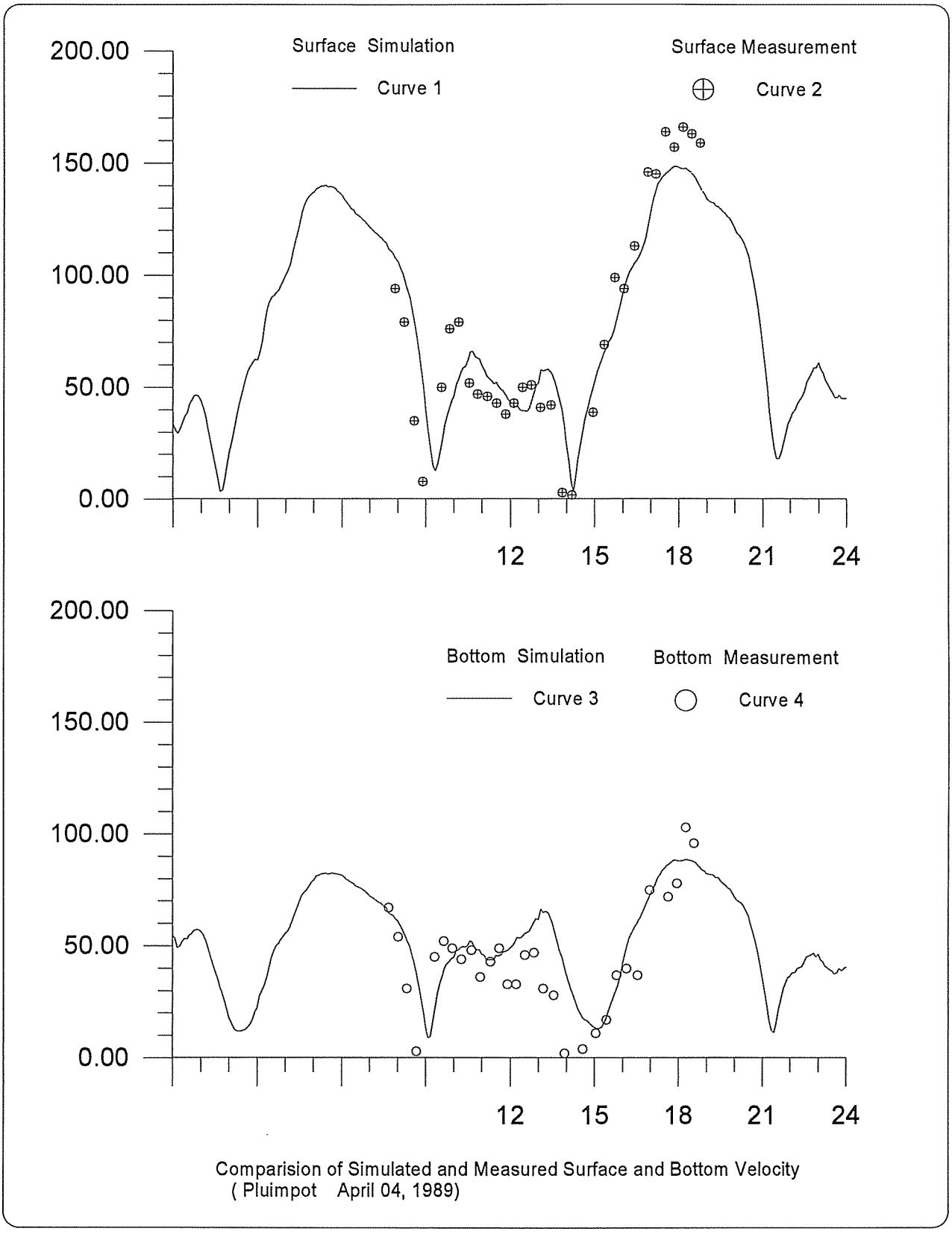

Figure 6-2: Comparison of simulated and measured surface and bottom current velocity on April 4 at station Pluimpot.

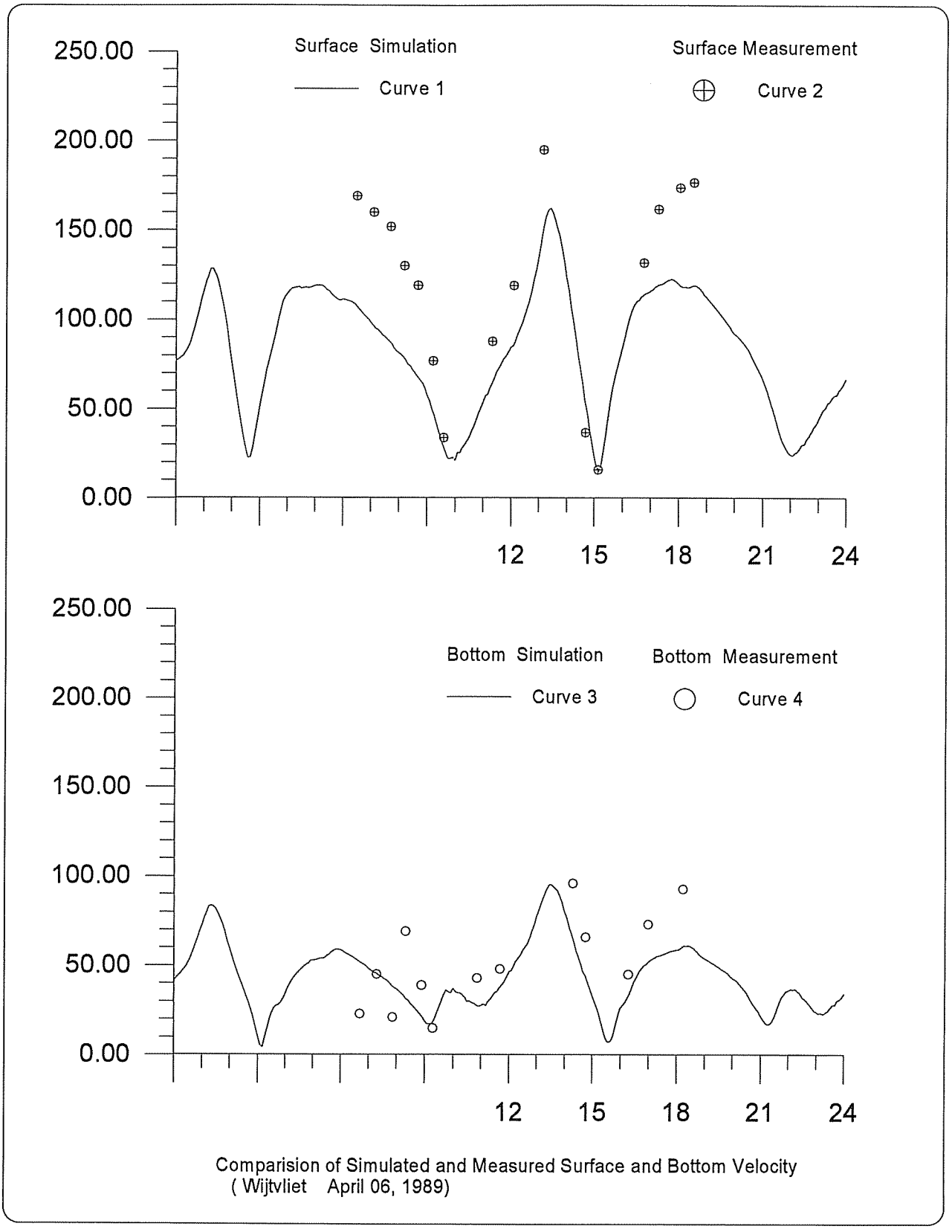

Figure 6-3: Comparison of simulated and measured surface and bottom current velocity on April 6 at station Wijtvliet.

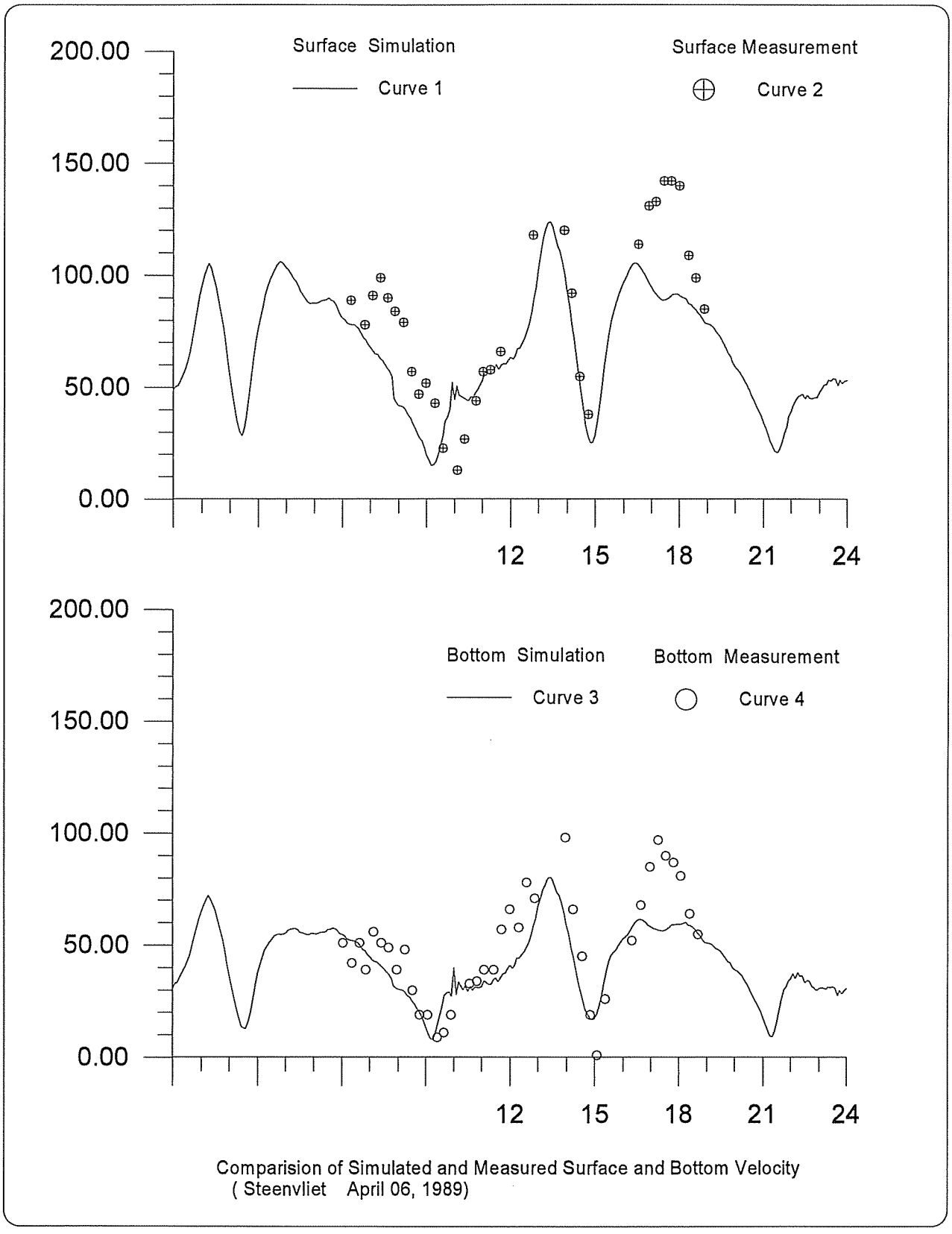

Figure 6-4: Comparison of simulated and measured surface and bottom current velocity on April 6 at station Steenvliet.

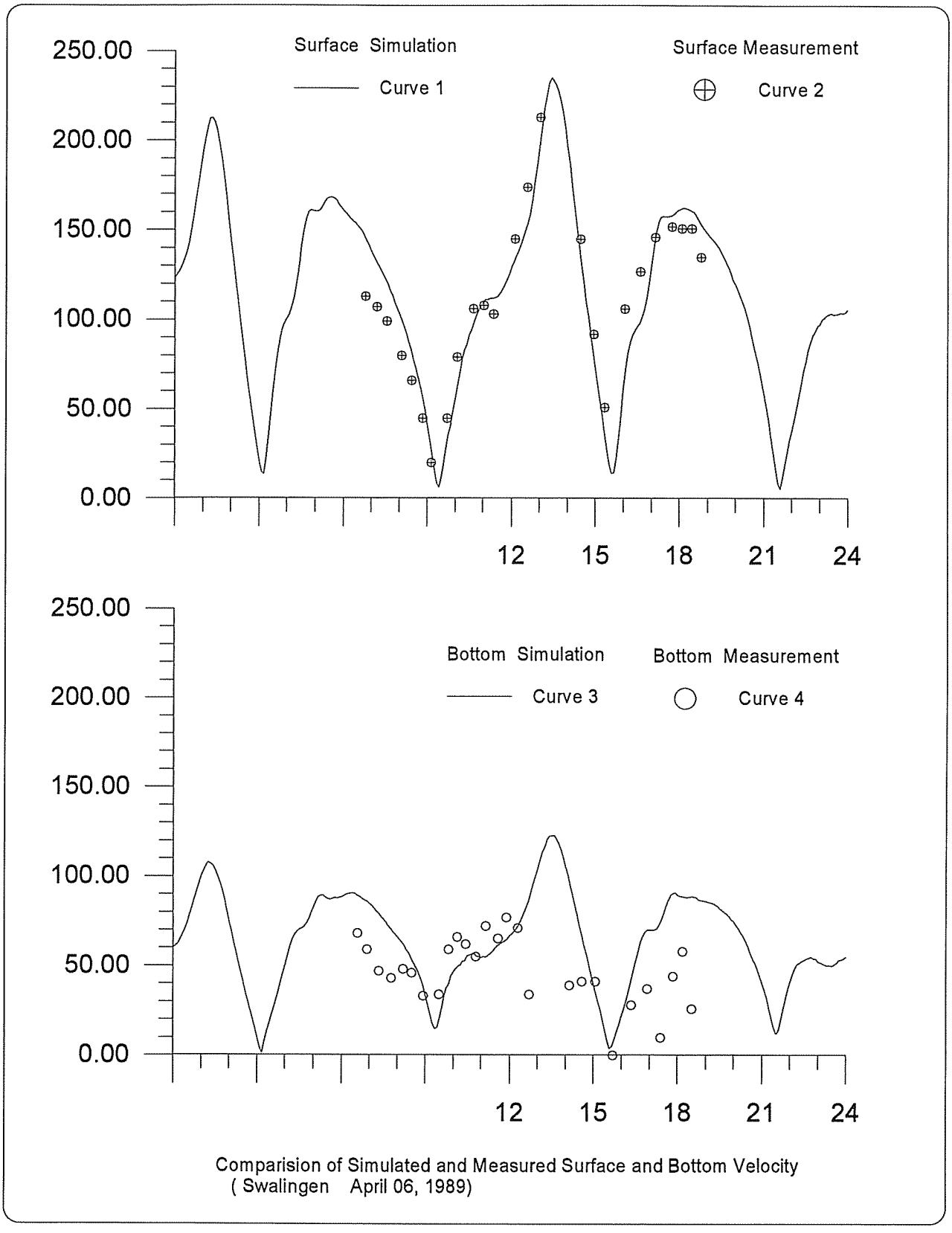

Figure 6-5: Comparison of simulated and measured surface and bottom current velocity on April 6 at station Swalinge.

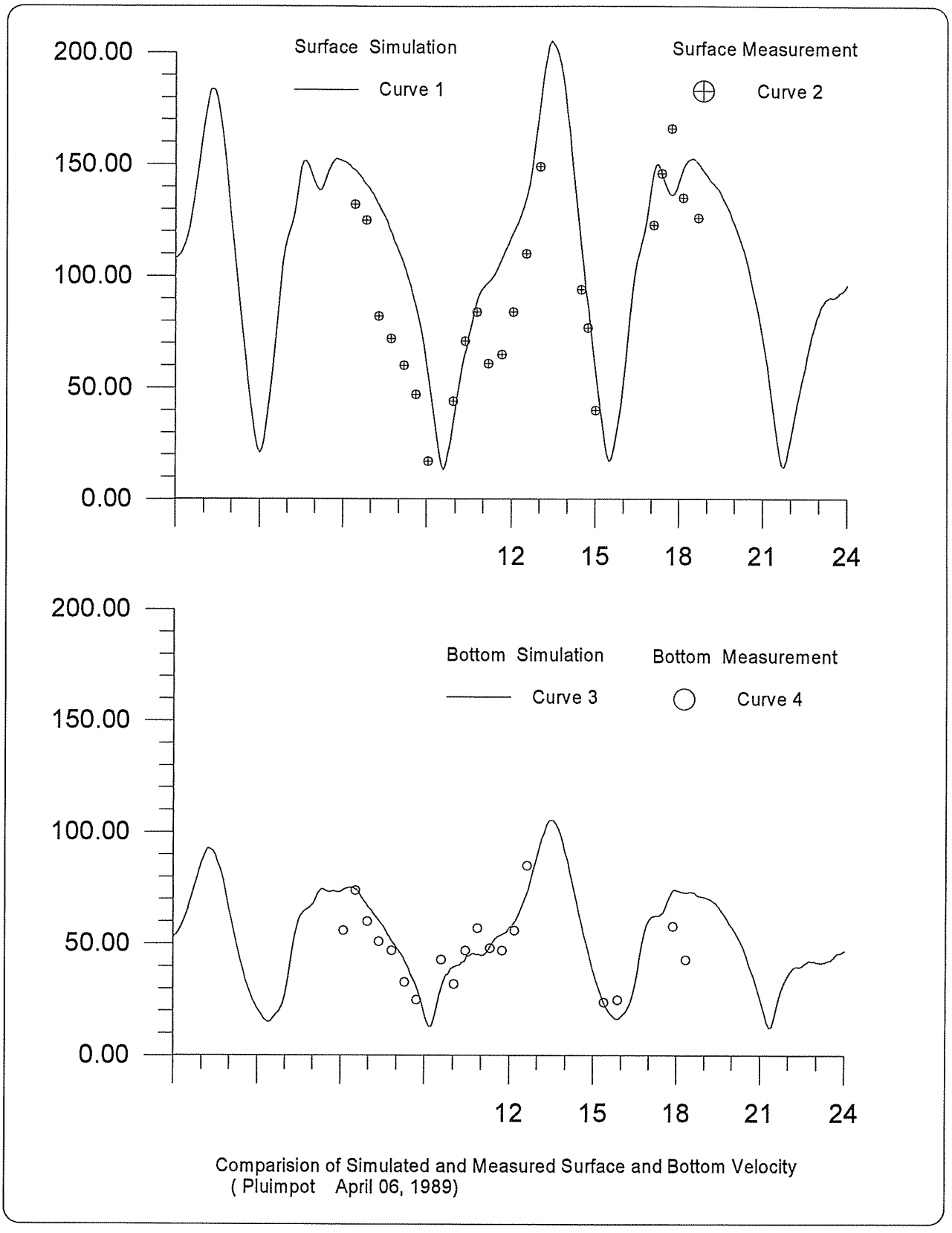

Figure 6-6: Comparison of simulated and measured surface and bottom current velocity on April 6 at station Pluimpot.

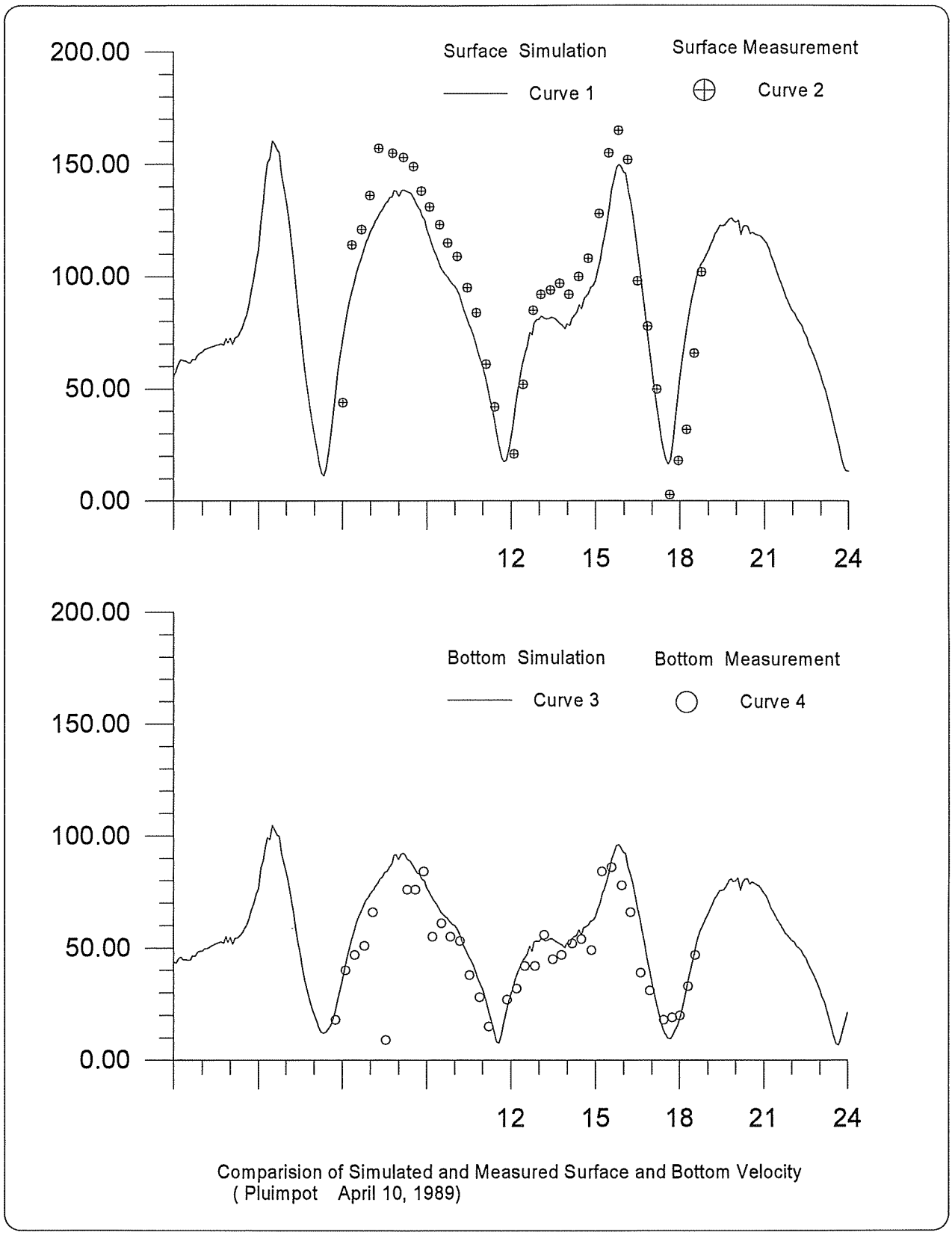

Figure 6-7: Comparison of simulated and measured surface and bottom current velocity on April 10 at station Pluimpot.

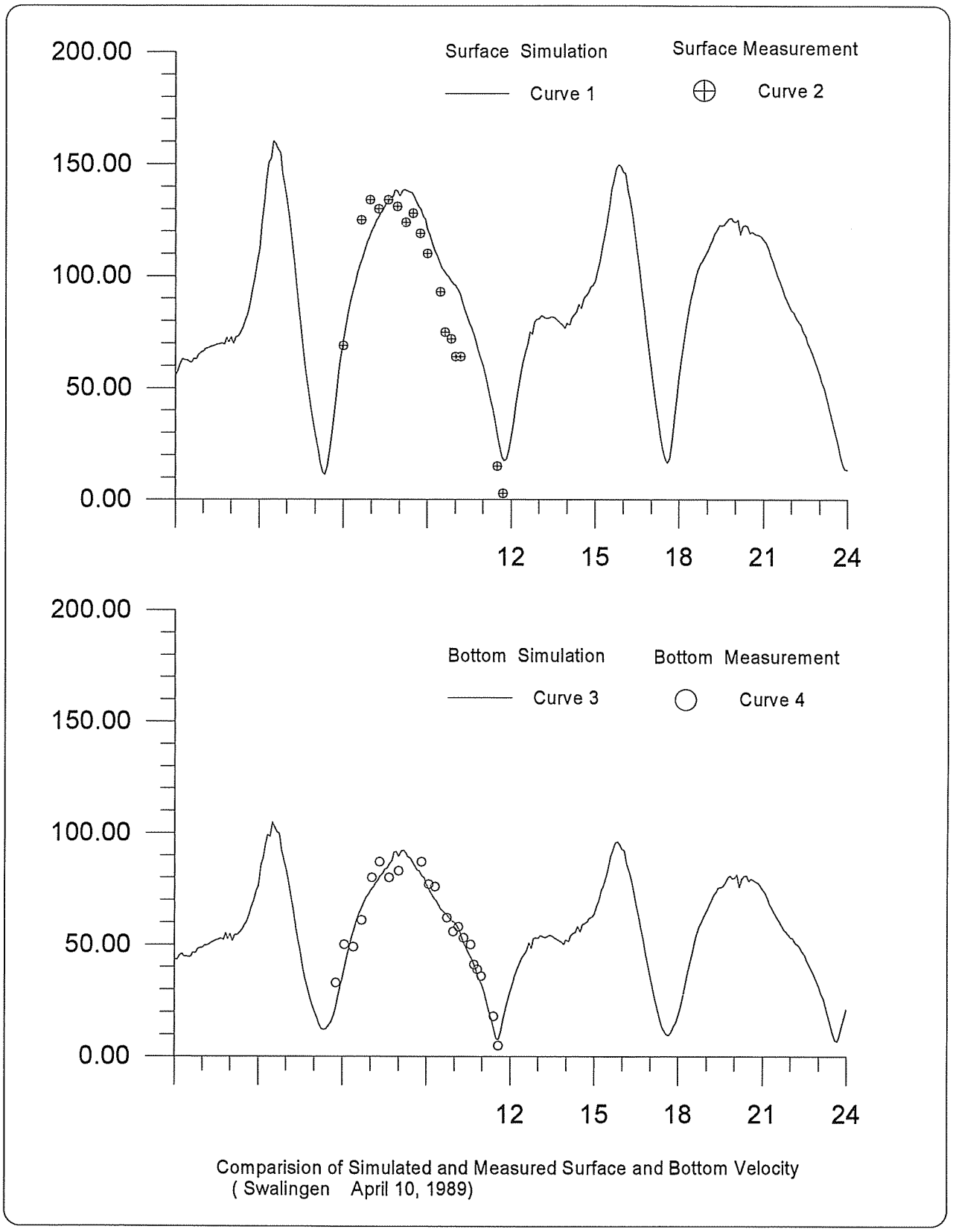

Figure 6-8: Comparison of simulated and measured surface and bottom current velocity on April 10 at station Swalinge.

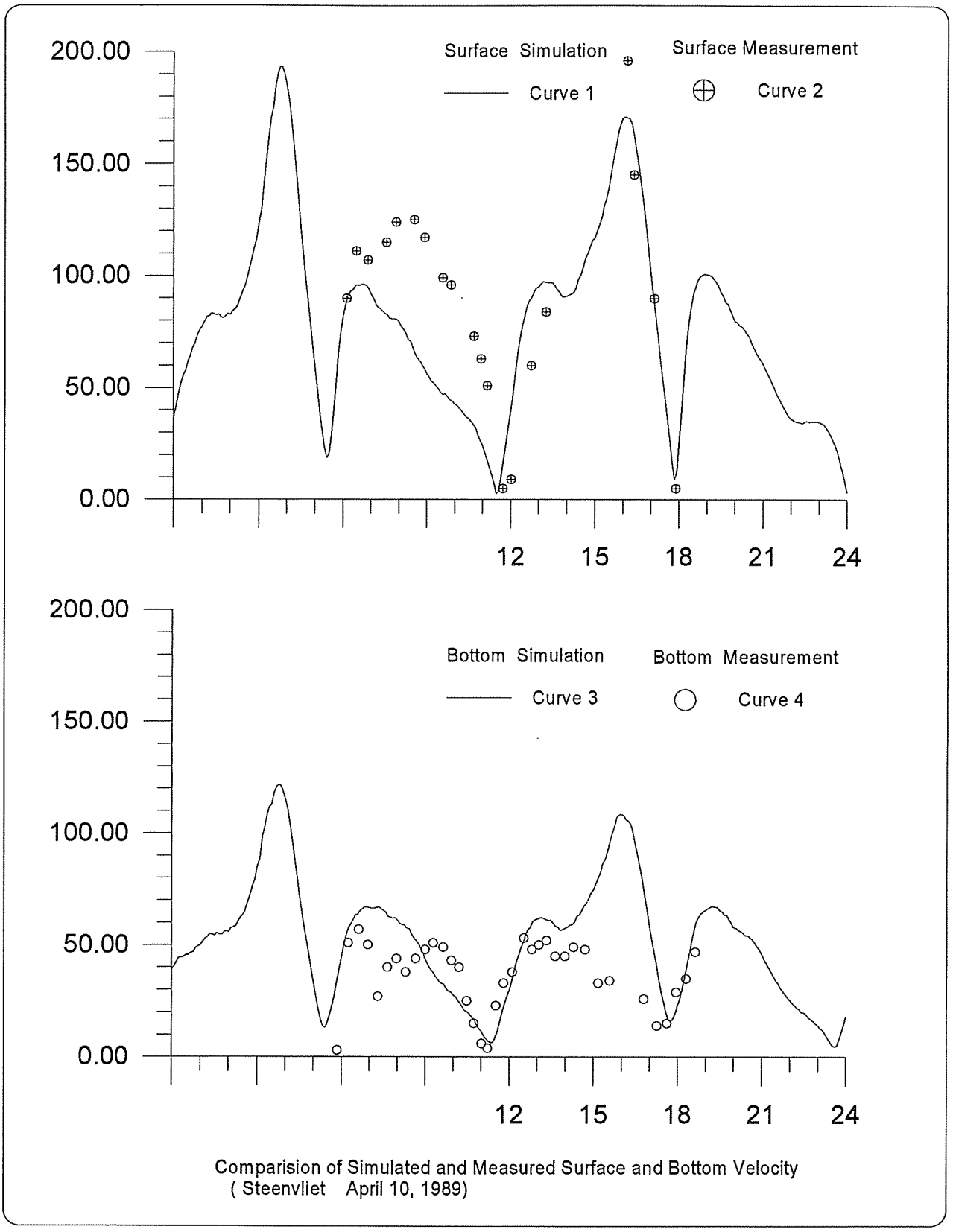

Figure 6-9: Comparison of simulated and measured surface and bottom current velocity on April 10 at station Steenvliet.

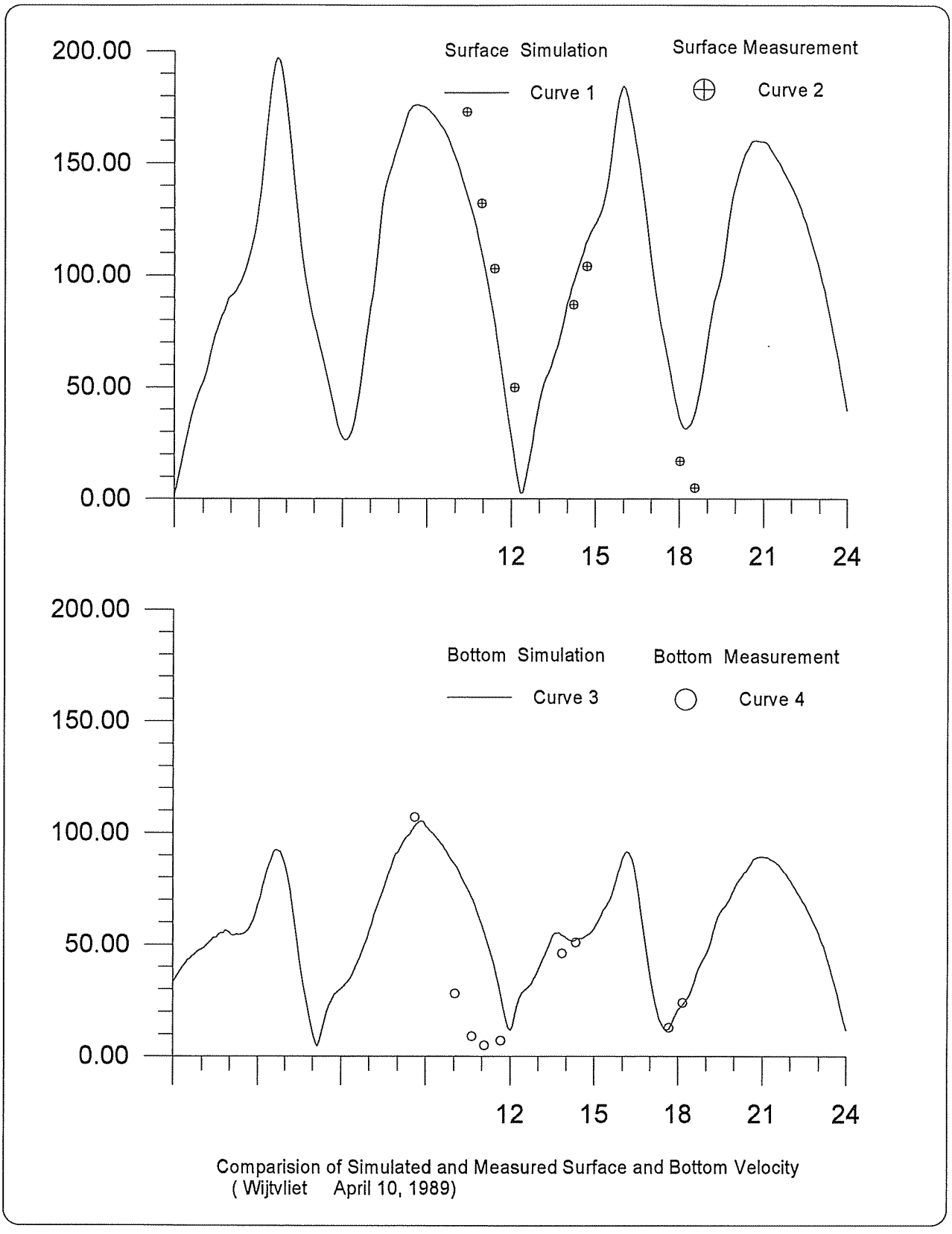

Figure 6-10: Comparison of simulated and measured surface and bottom current velocity on April 10 at station Wijtvliet.

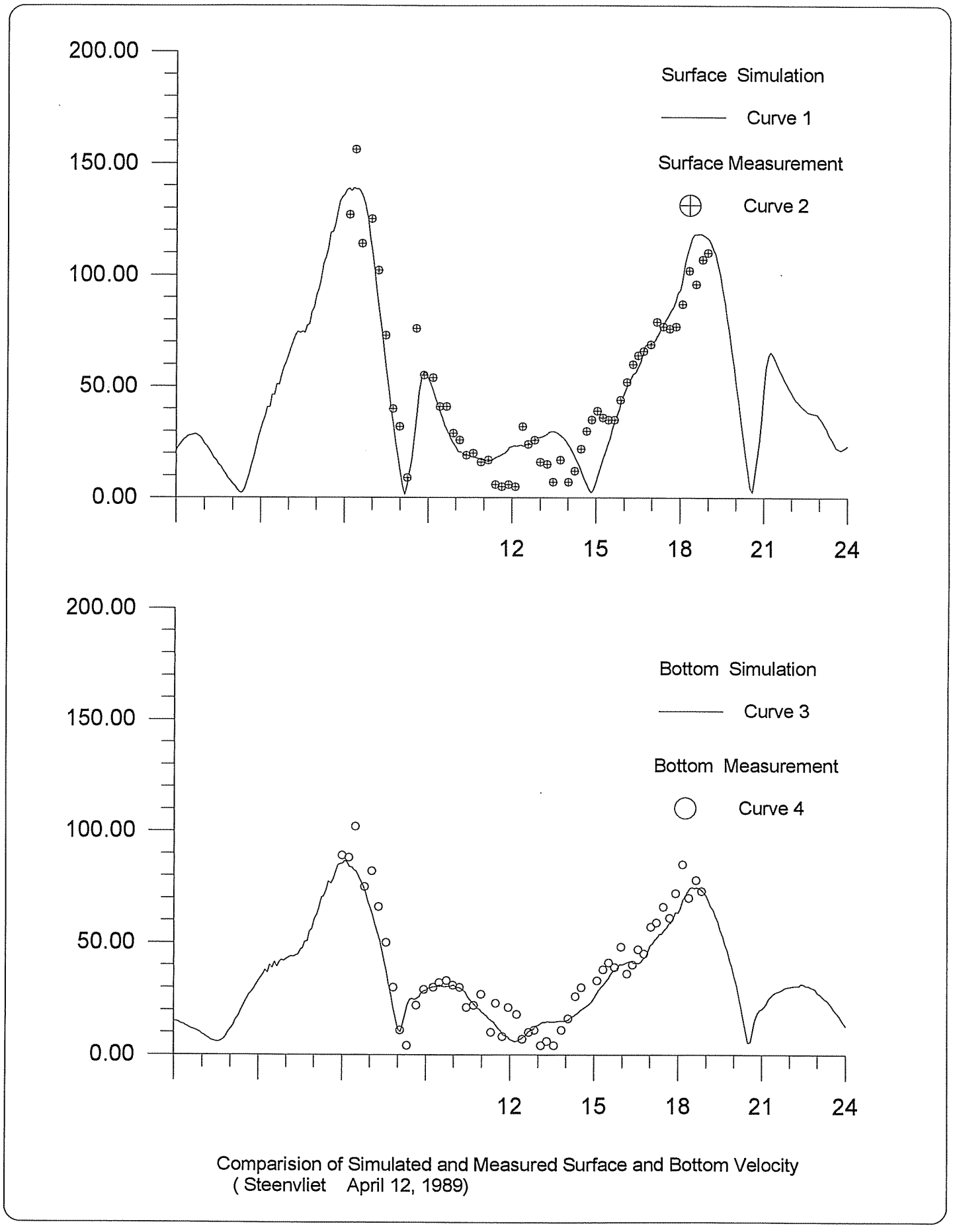

Figure 6-11: Comparison of simulated and measured surface and bottom current velocity on April 12 at station Steenvliet.

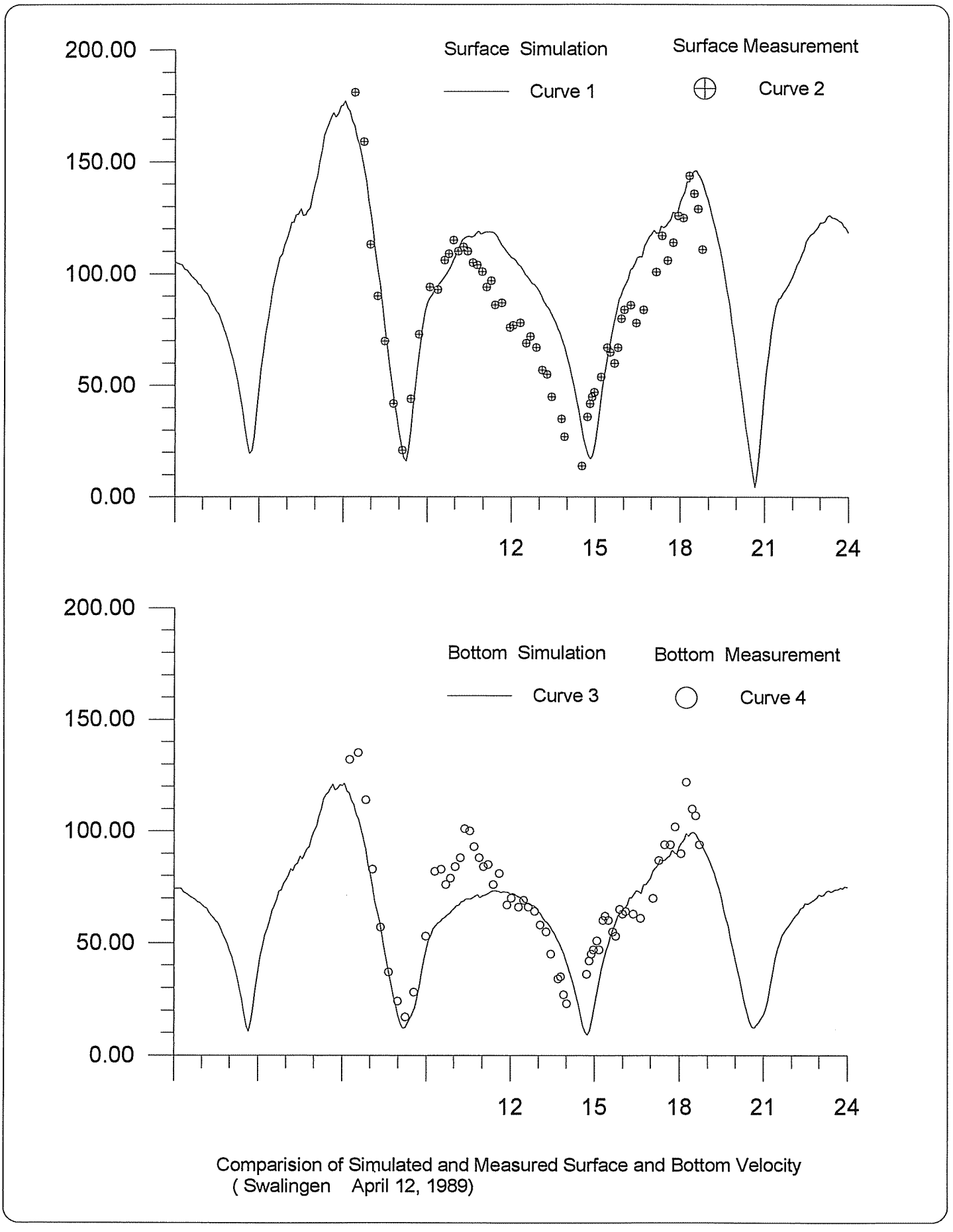

Figure 6-12: Comparison of simulated and measured surface and bottom current velocity on April 12 at station Wijtvliet.

Figure 7-1: Surface current velocity on April 12 from 9.00 until 14.00.

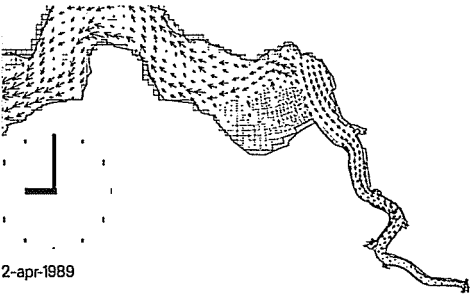

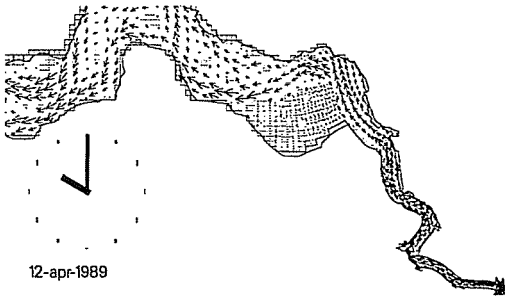

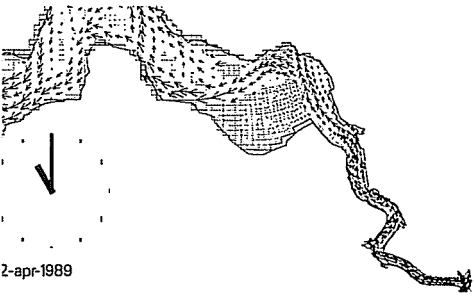

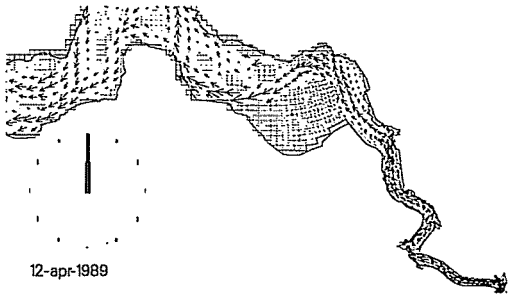

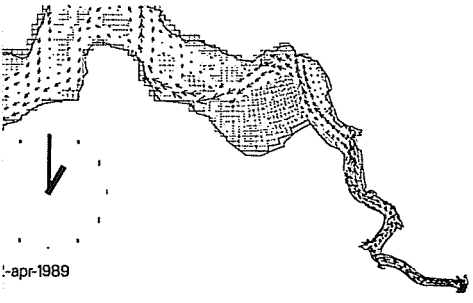

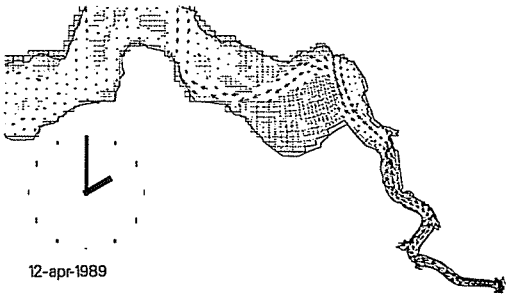

gure 7-2: Surface current velocity on April 12 from 15.00 until 20.00.

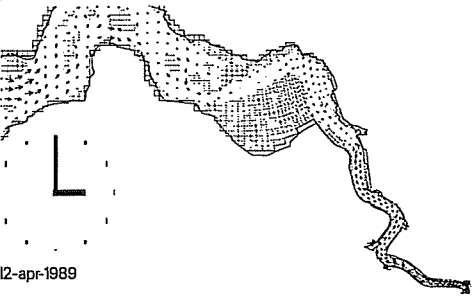

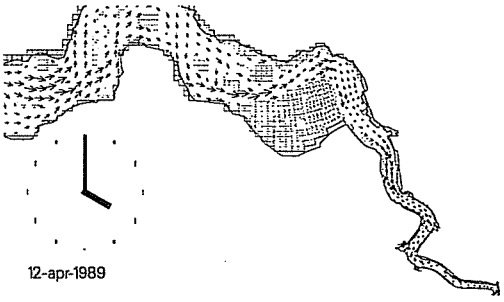

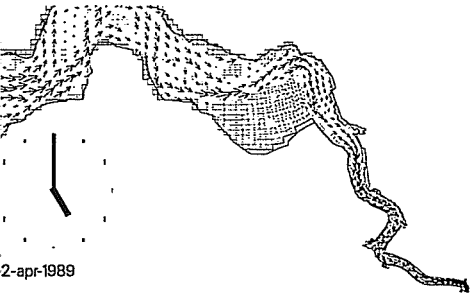

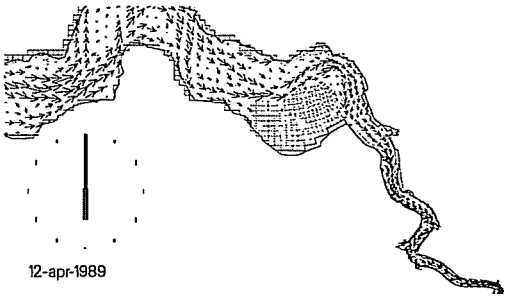

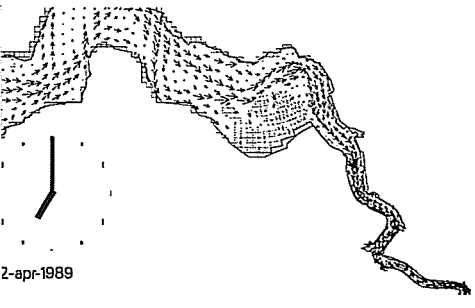

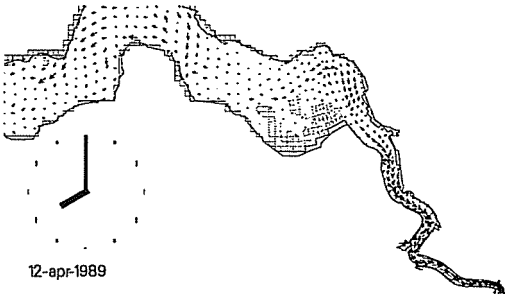

Figure 7-3: Bottom current velocity on April 12 from 9.00 until 14.00.

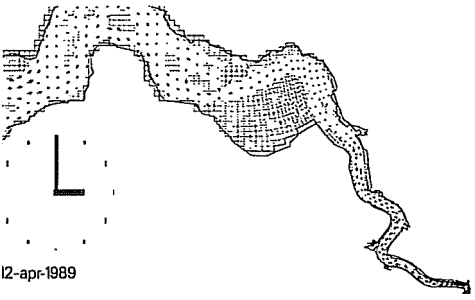

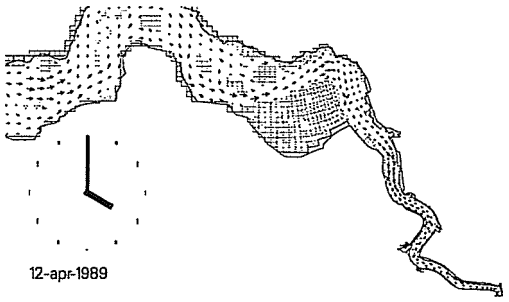

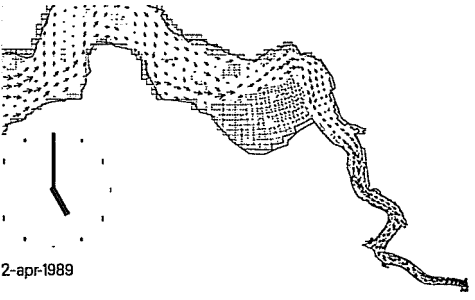

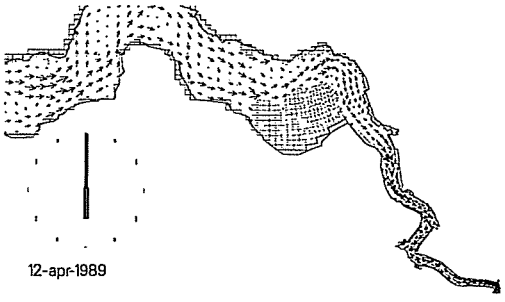

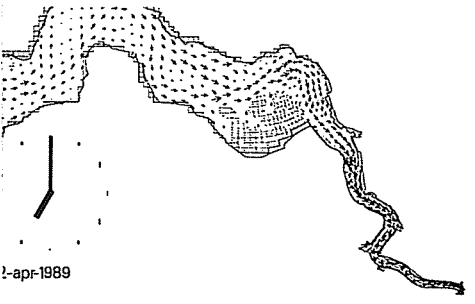

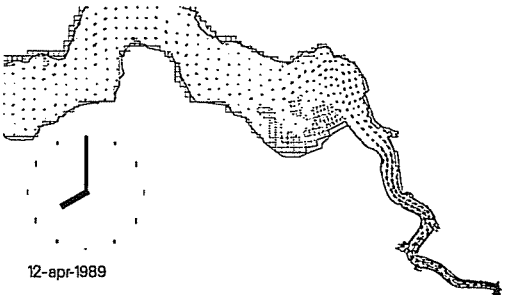

Figure 7-4: Bottom current velocity on April 12 from 15.00 until 20.00.

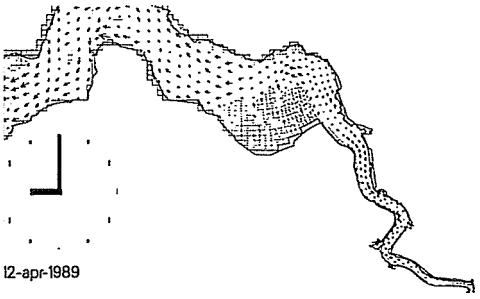

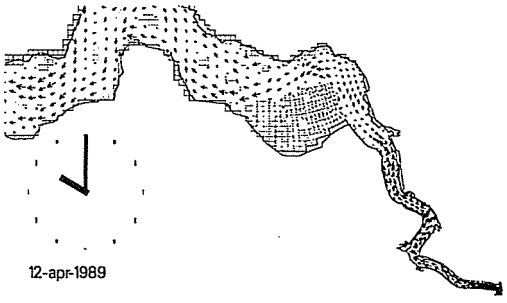

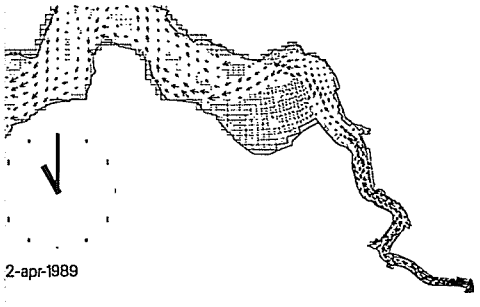

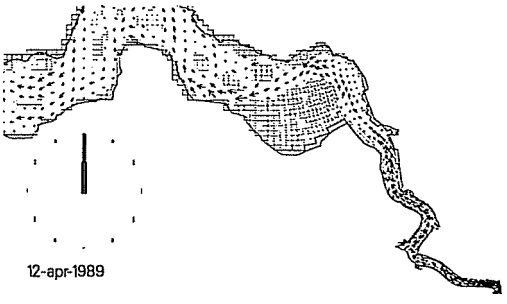

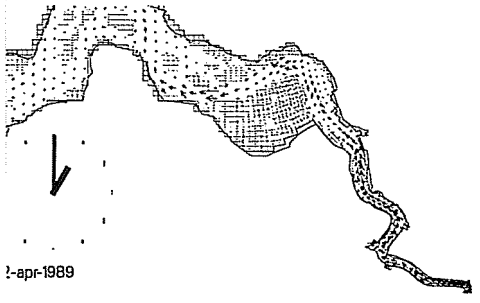

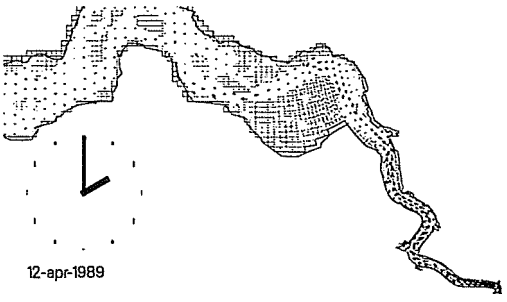

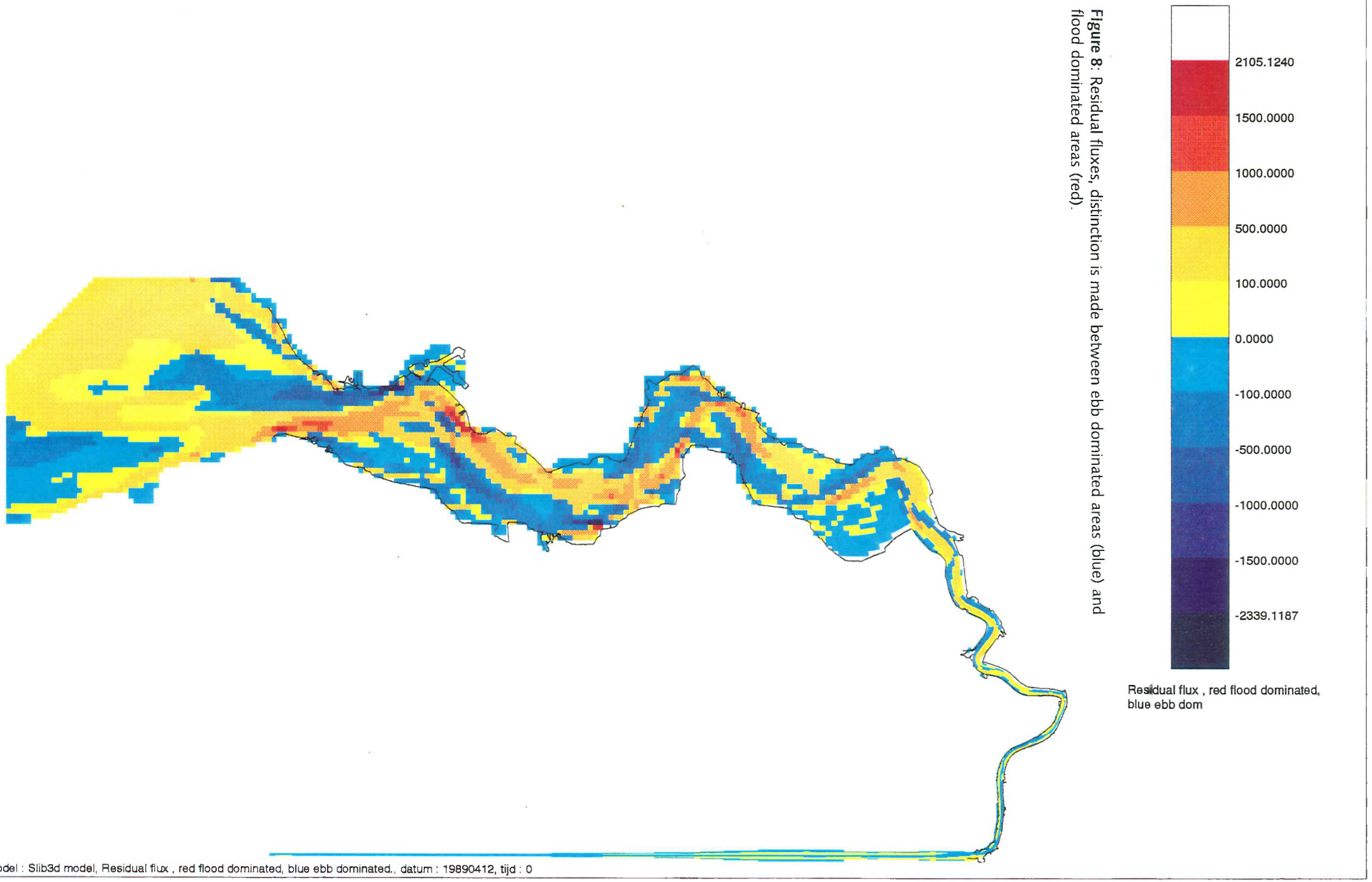

Figure 8: Residual fluxes, distinction is made between ebb dominated areas (blue) and flood dominated areas (red).

Figure 9: Surface and bottom current velocity and low water.

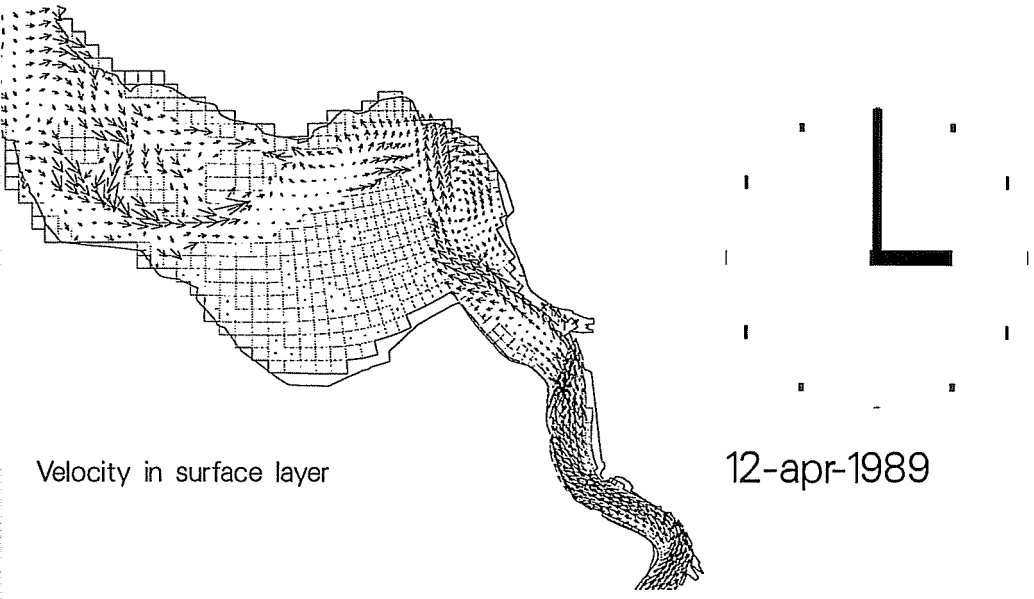

Velocity in surface layer

12-apr-1989

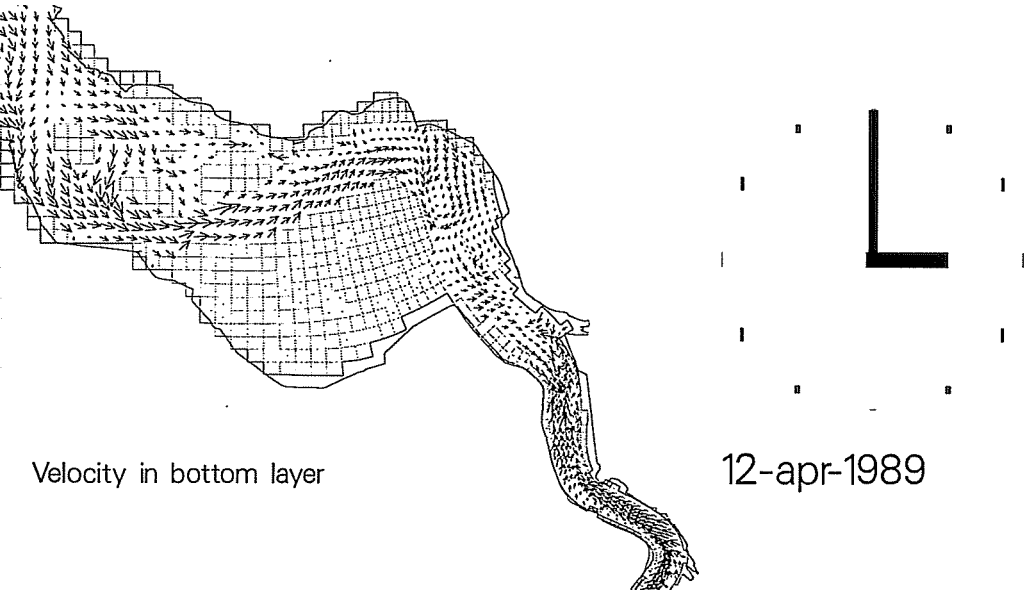

Velocity in bottom layer

12-apr-1989

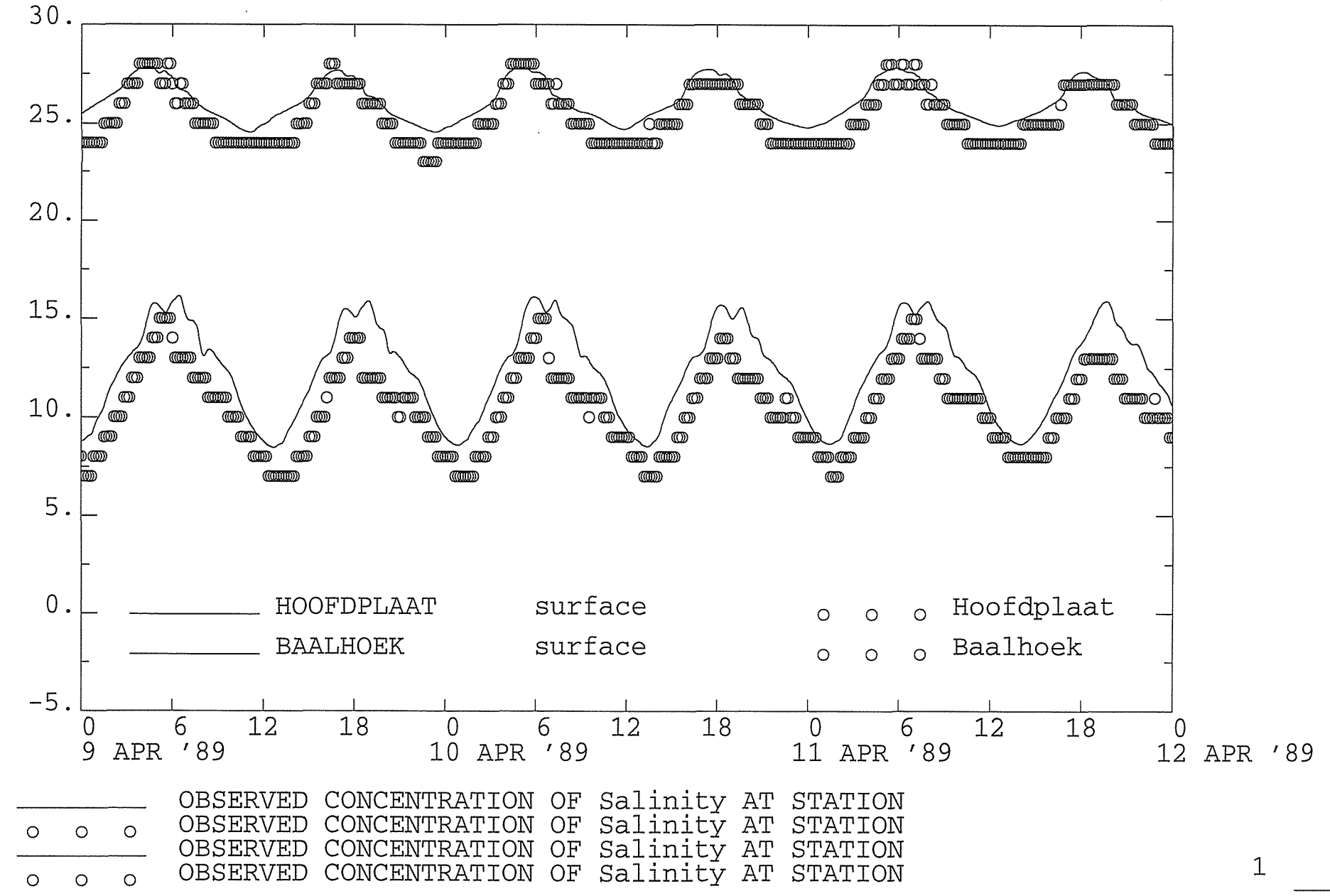

Figure 10-1: Measured versus modelled surface salinity at stations Hoofdplaat and Baalhoek.

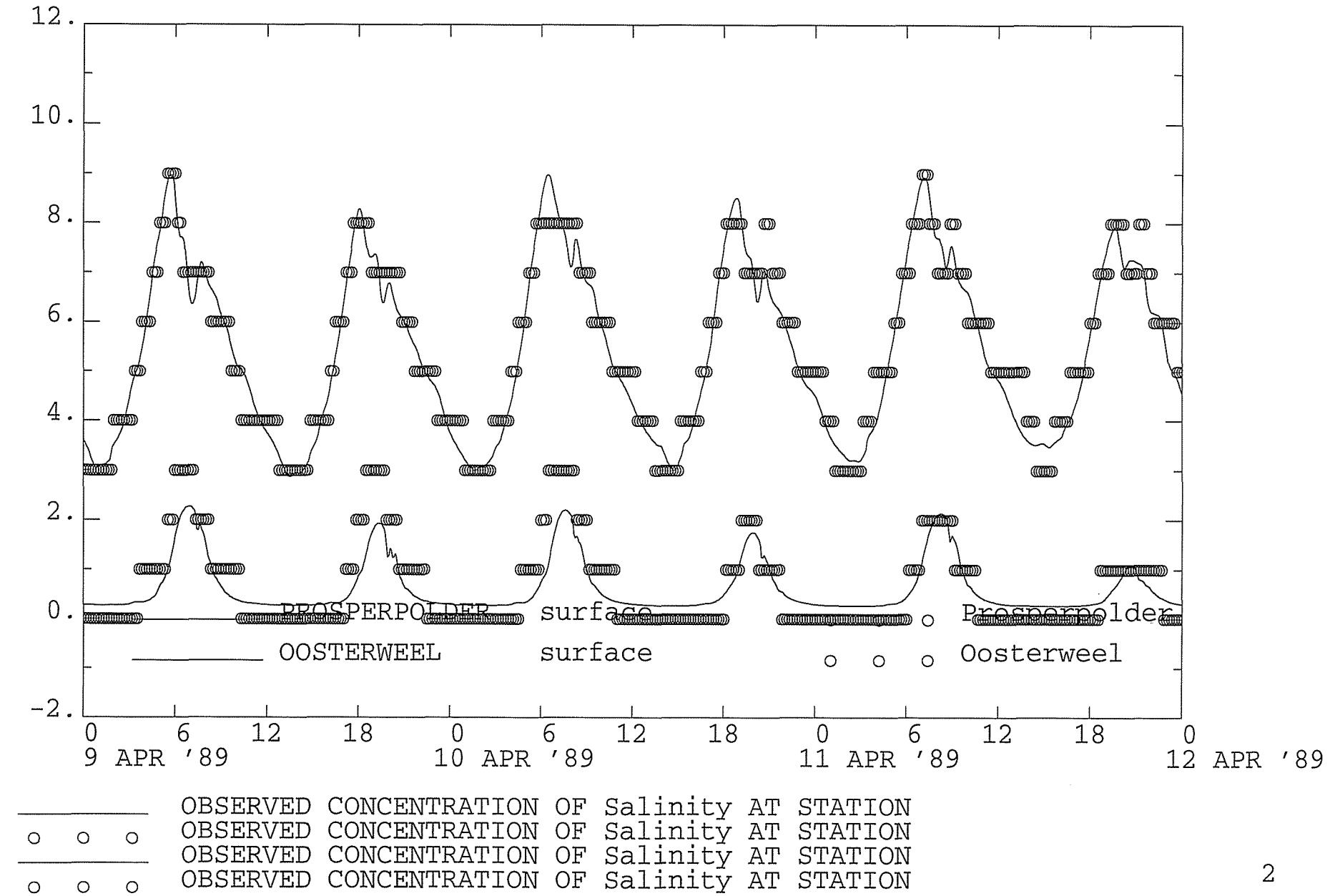

Figure 10-2: Measured versus modelled surface salinity at stations Prosperpolder and Oosterweel.

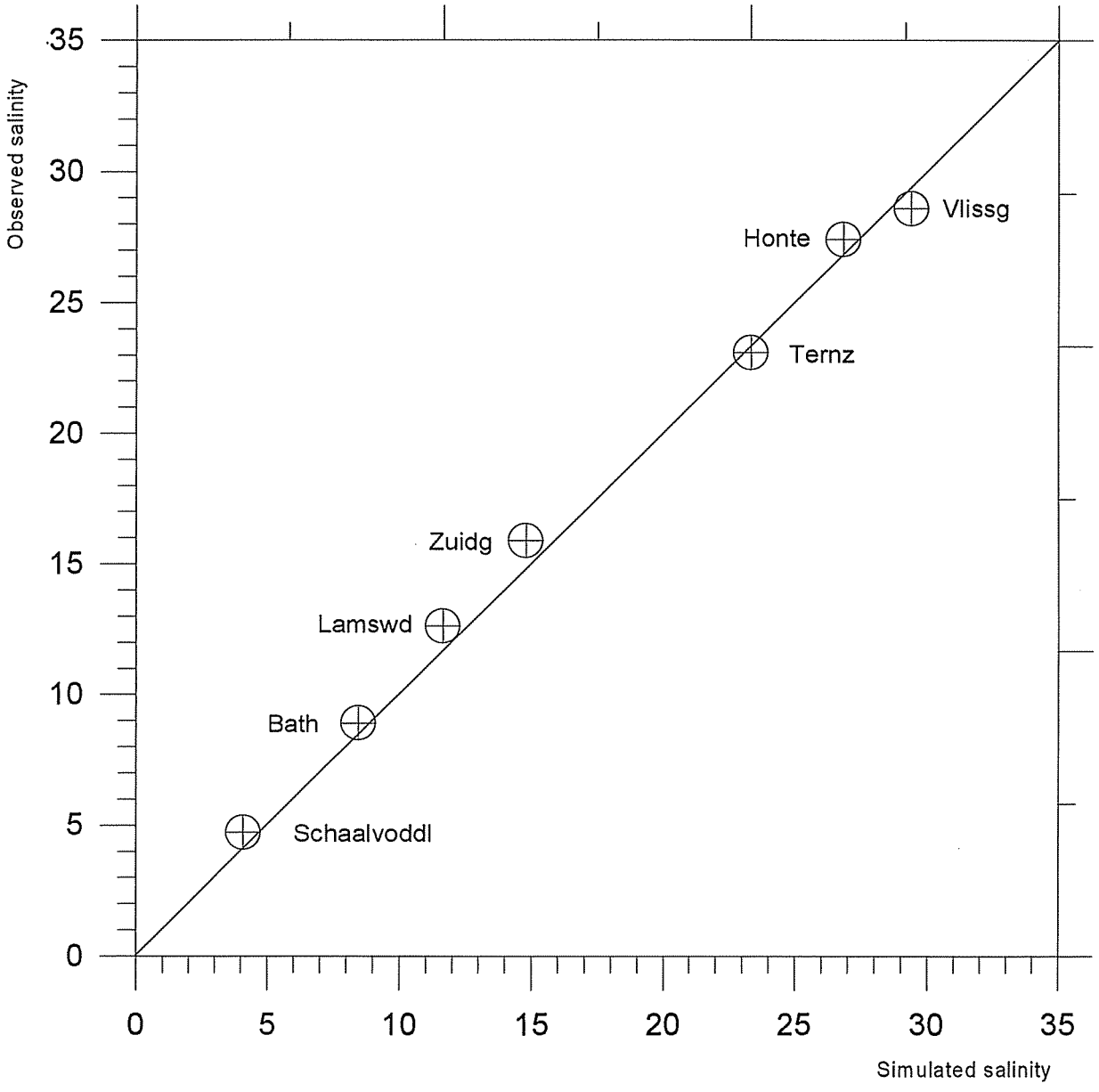

Figure 11: Measured versus modelled surface salinity at 7 locations in the Scheldt estuary.

Figure 12-1: Evolution of surface salinity on April 12 from 9.00 until 14.00.

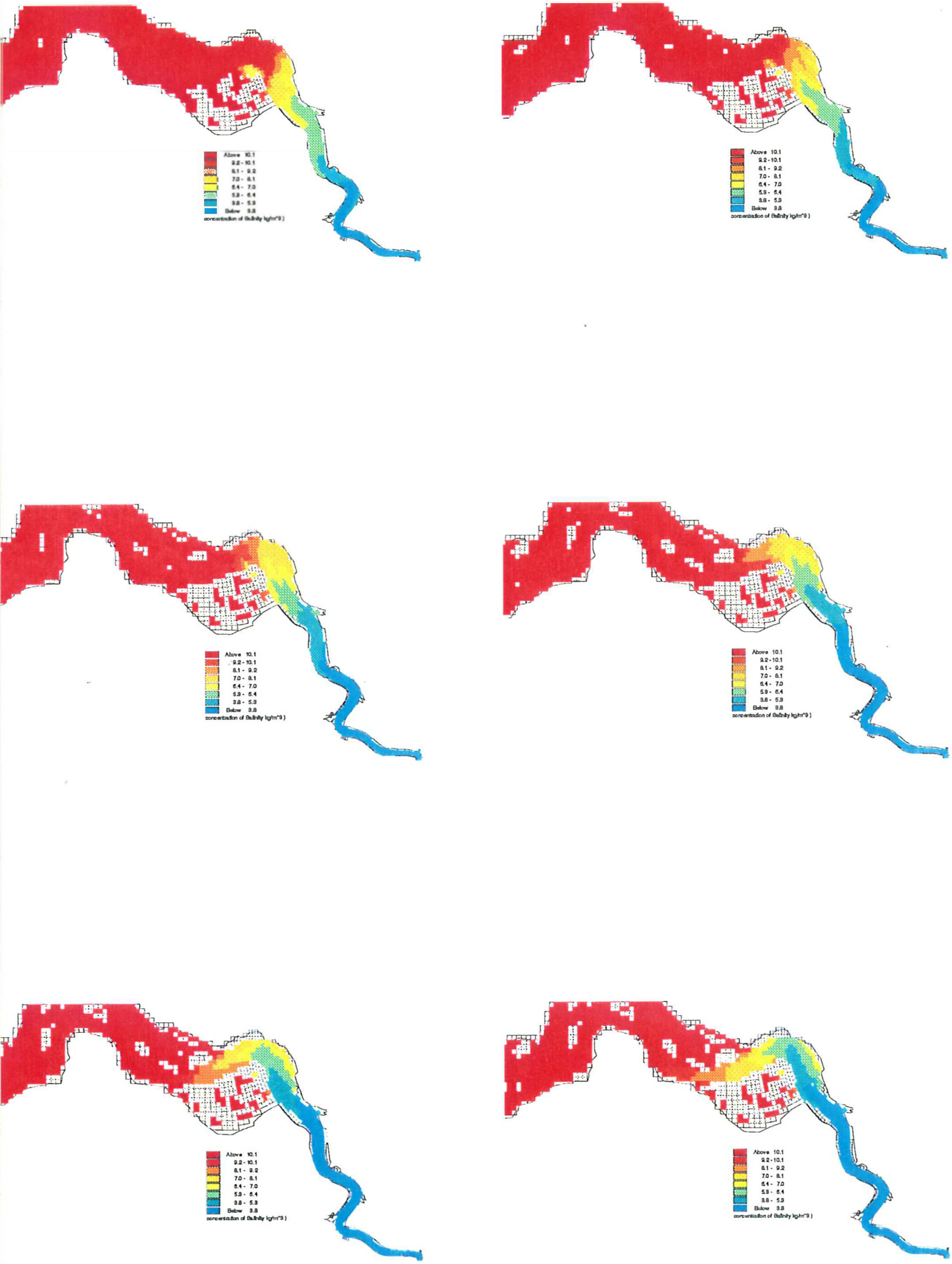

Figure 12-2: Evolution of bottom salinity on April 12 from 9.00 until 14.00.

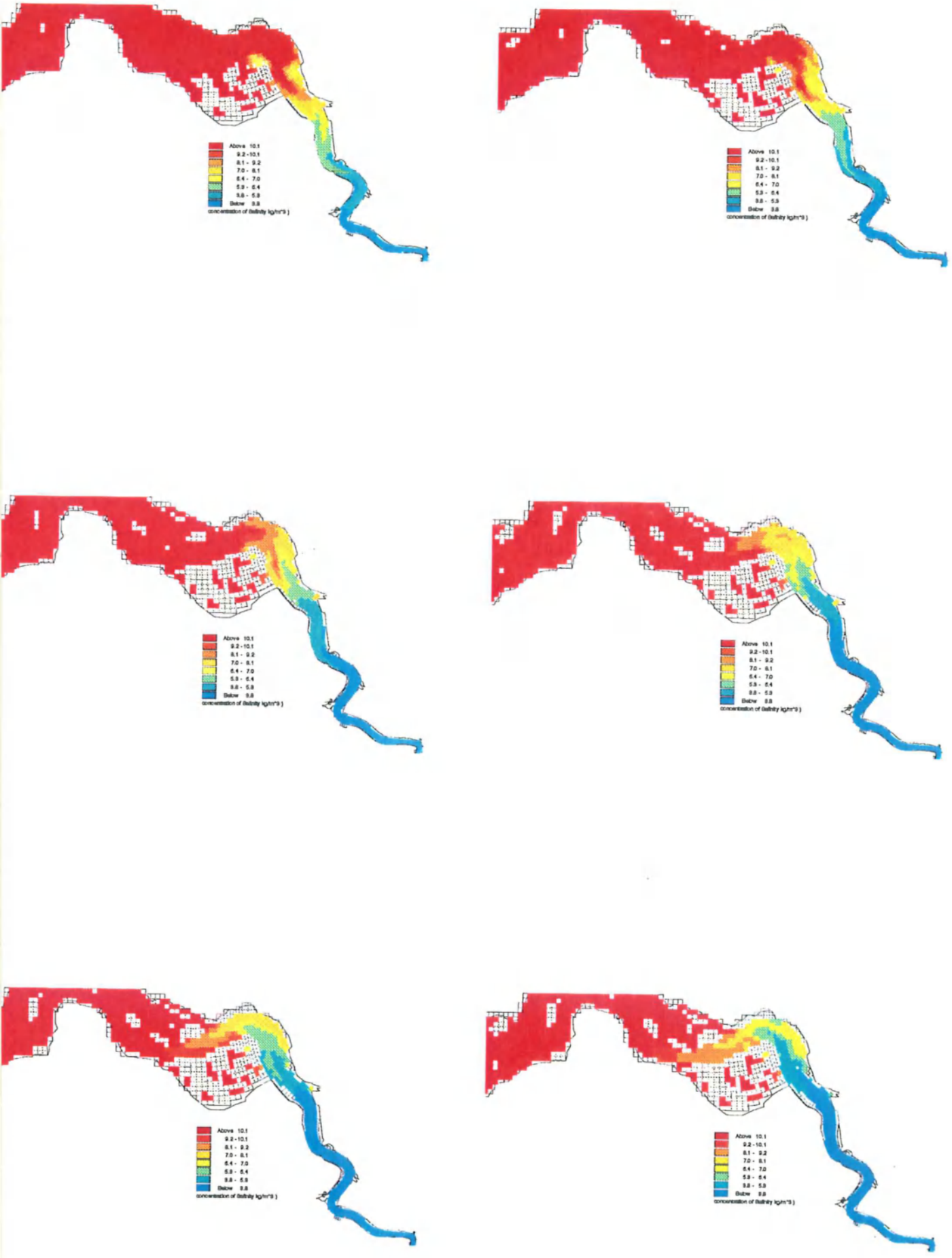

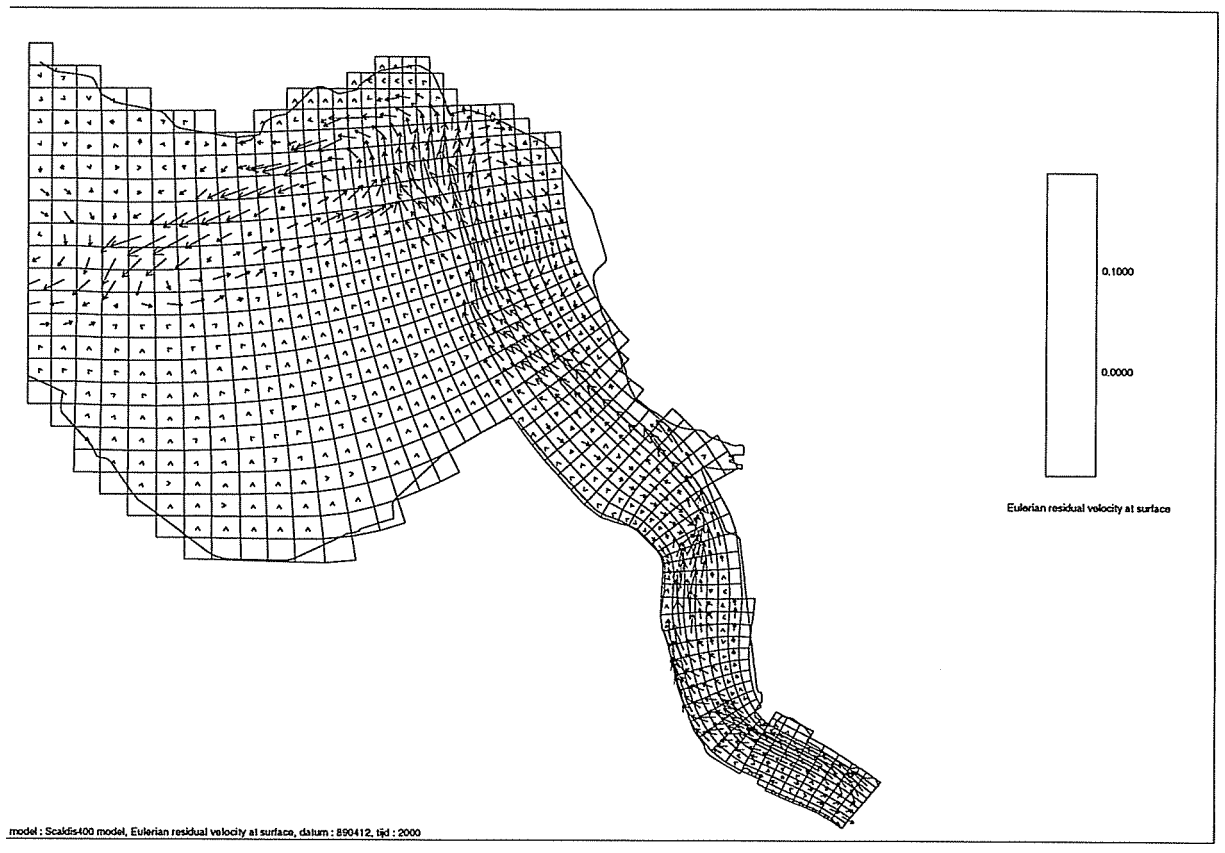

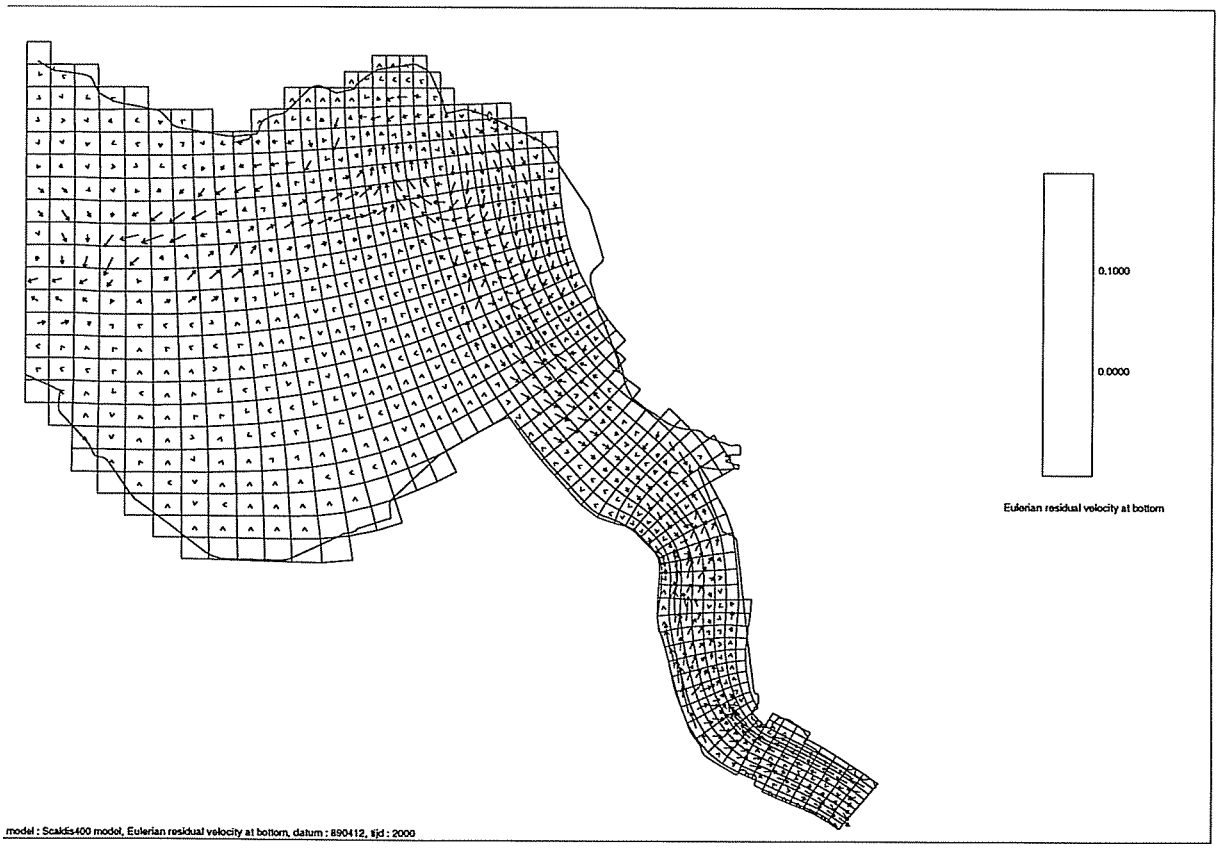

Figure 13-1: Eulerian residual circulation at the surface (top) and bottom (down) on April 12 near Bath.

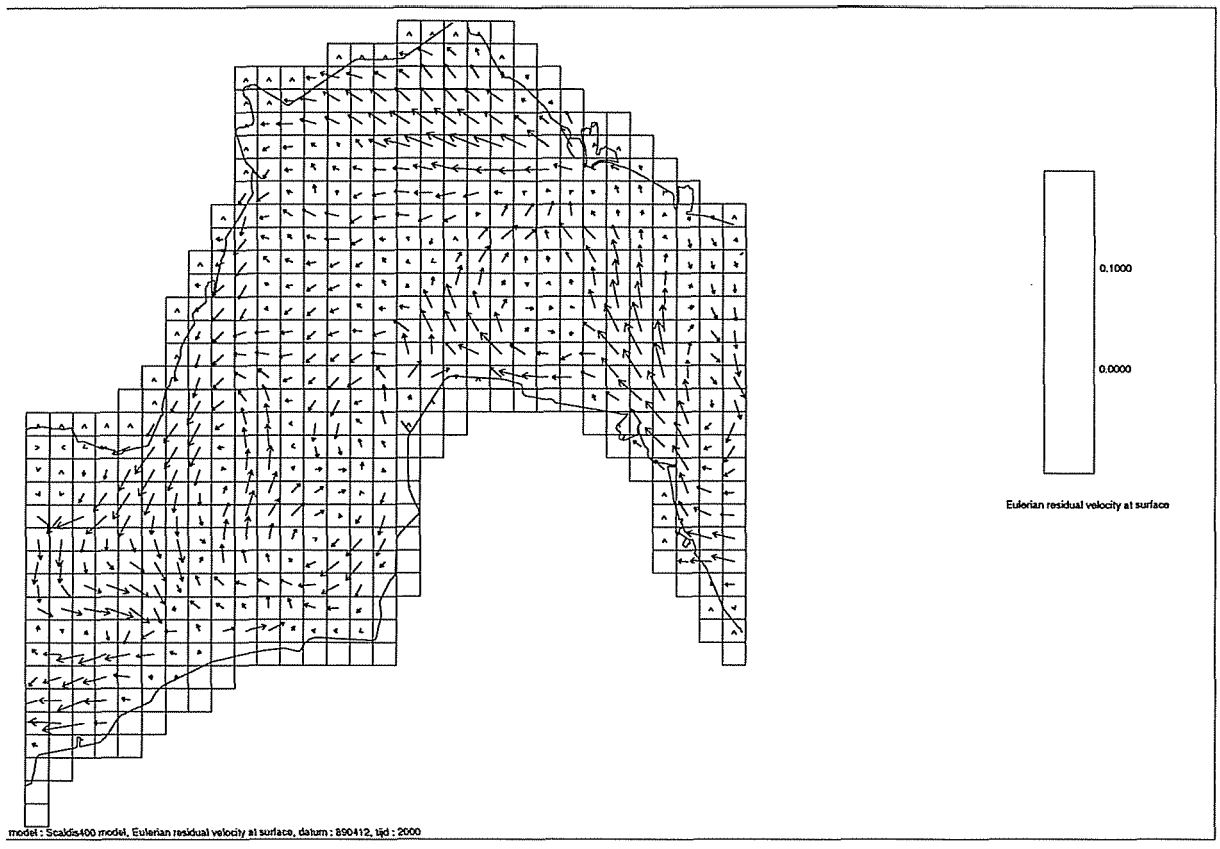

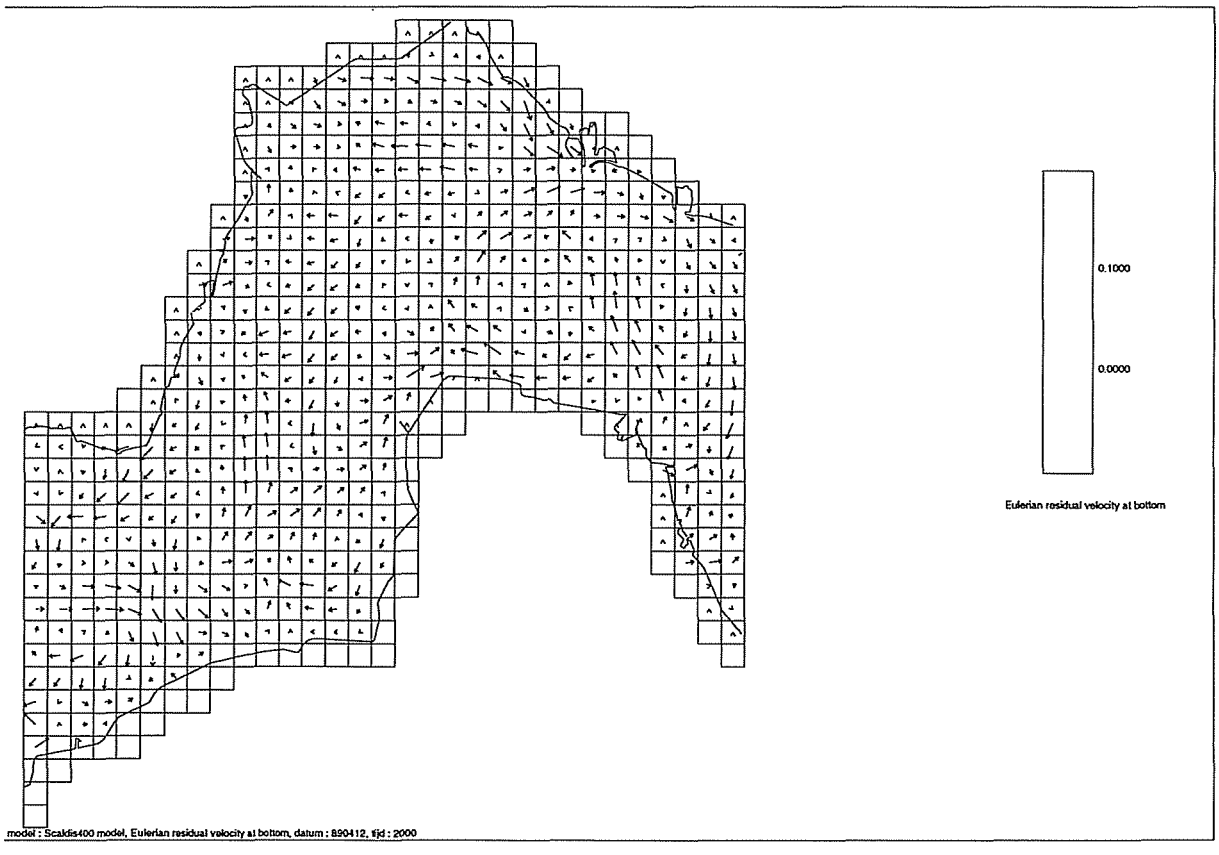

Figure 13-2: Eulerian residual circulation at the surface (top) and bottom (down) on April 12 near Hansweert.